Variability in Low Ionization Broad Absorption Line outflows

M. Vivek, R. Srianand, P. Petitjean, V. Mohan, A. Mahabal, S. Samui

Variability in Low Ionization Broad Absorption Line outflows

M. Vivek,[1]⋆ R. Srianand,[1] P. Petitjean,[2] V. Mohan,[1] A. Mahabal[3] and S. Samui[4]

[1]*Inter-University Centre for Astronomy and Astrophysics, Post bag 4, Ganeshkhind, Pune 410007, India*
[2]*UPMC-CNRS, UMR7095, Institut d′Astrophysique de Paris, 98bis Boulevard Arago, F-75014 Paris, France*
[3]*Caltech, MC 249-17, Pasadena, CA 91125, USA*
[4]*Department of Physics, Presidency University, 86/1 College Street, Kolkata 700073, India*

ABSTRACT

We present results of our time variability studies of Mg II and Al III absorption lines in a sample of 22 Low Ionization Broad Absorption Line QSOs (LoBAL QSOs) at $0.2 \leq z_{em} \leq 2.1$ using the 2-m telescope at IUCAA Girawali Observatory over a time-scale of 10 d to 7.69 years in the QSO's rest frame. Spectra are analysed in conjunction with photometric light curves from Catalina Real-Time Transient Survey. Long time-scale (i.e. ≥ 1 year) absorption line variability is seen in eight cases (36 per cent systems) while only four of them (i.e. 18 per cent systems) show variability over short time-scales (i.e. <1 year). We notice a tendency of highly variable LoBAL QSOs to have high ejection velocity, low equivalent width and low redshift. The detection rate of variability in LoBAL QSOs showing Fe fine-structure lines (FeLoBAL QSOs) is less than that seen in non-Fe LoBAL QSOs. Absorption line variability is more frequently detected in QSOs having continuum dominated by Fe emission lines compared to rest of the QSOs. Confirming these trends with a bigger sample will give vital clues for understanding the physical distinction between different BAL QSO sub-classes. We correlate the absorption line variability with various parameters derived from continuum light curves and find no clear correlation between continuum flux and absorption line variabilities. However, sources with large absorption line variability also show large variability in their light curves. We also see appearance/disappearance of absorption components in two cases and clear indications for profile variations in four cases. The observed variability can be best explained by a combination of process driven by continuum variations and clouds transiting across the line of sight.

Key words: galaxies: active – quasars: absorption lines – quasars: general.

1 INTRODUCTION

In recent years, the importance of understanding the nature and origin of QSO outflows has become widely recognized in the context of well-studied correlations between the Super Massive Black Hole (SMBH) and host galaxy properties (Silk & Rees 1998; Ferrarese & Merritt 2000). The inferred kinetic luminosities of these outflows suggest that they could in principle be a major contributor to the active galactic nuclei (AGN) feedback mechanisms (Moe et al. 2009; Dunn et al. 2010; Bautista et al. 2010; Aoki et al. 2011; Borguet et al. 2012, 2013). QSO outflows are also an important diagnostic of the physical conditions and chemical enrichment prevailing in the inner regions of the AGNs.

QSO outflows are readily identified as blue shifted broad absorption lines (BAL) seen in 10–40 per cent of the total quasars (Hewett & Foltz 2003; Reichard et al. 2003; Trump et al. 2006; Allen et al. 2011; Pâris et al. 2012). By definition, BAL QSOs are characterized by absorption troughs which dip by more than 10 per cent below the continuum for a contiguous stretch of at least $2000\,\mathrm{km\,s^{-1}}$ and extend up to velocities ~ 0.2 c with respect to the systemic redshift (Weymann et al. 1991). BAL QSOs are further divided in three sub-types depending on the type of transition seen in absorption. Most of the known BAL QSOs are high ionization BALs (HiBALs) characterized by absorptions from C IV, Si IV, N V, and Lyα. About 15 per cent are Low ionization BALs (LoBAL QSOs) which exhibit absorption lines of Mg II, Al II, Al III and sometimes Fe II and Fe III in addition to the above listed high ionization absorption lines. The rarer (~ 1 per cent) iron LoBAL QSOs (FeLoBAL QSOs) also show absorption from excited fine-structure levels of Fe II or Fe III. Recently thanks to the cosmic origin spectrograph on-board *HST*

⋆ E-mail: vivekm@iucaa.ernet.in

(COS/*HST*), outflows traced by very highly ionized species like Ne VII, Mg X and Na X have been detected in ~40 per cent of low-z QSOs (Muzahid et al. 2012, 2013). The observed BAL incidence is attributed to either an orientational effect where the observer's line of sight passes through the BAL clouds or an evolutionary phase in the QSO lifetime or a combination of the two.

Even though recent spectroscopic surveys have dramatically increased the number of known BAL QSOs, still there is no commonly accepted model which explains the geometry and the physical properties of the outflows. Line-driven radiative acceleration is suggested based on spectroscopic signatures (Arav, Li & Begelman 1994; Arav et al. 1995; Srianand et al. 2002). de Kool & Begelman (1995) proposed a model in which gas is clumped in small clouds confined by magnetic pressure and driven by radiation-pressure. There is another dynamical model which assumes outflows as winds streaming out of the accretion-disc at a distance $R \sim 10^{16}$ cm and driven by the radiative UV line pressure (Murray et al. 1995; Proga, Stone & Kallman 2000; Elvis 2000). The proposed 'shielding gas' absorbs the X-rays from the quasar and protects the wind from being completely ionized, also explains the observed X -ray weakness of BAL QSOs (see Green et al. 1995; Gallagher et al. 2006; Fan et al. 2009; Gibson et al. 2009; Stalin, Srianand & Petitjean 2011). Most current models favour the equatorial geometry of the BAL outflows although after the discovery of radio loud BAL QSOs (Becker et al. 1997, 2000) polar outflows have been suggested for some of them (Ghosh & Punsly 2007). A two-component wind model combining the polar and equatorial components has also been suggested to explain the polar outflows (Lamy & Hutsemékers 2004; Proga & Kallman 2004; Borguet & Hutsemékers 2010). The exact geometry of the BAL outflows is still under theoretical and observational investigation.

As the launching radii of the winds in some models are very close to the QSO central engine, instabilities in the accretion disc can result in variations in the outflow properties on time-scales of a few years. Thus, BAL variability studies are important to understand the location and physical conditions in the absorbing gas and the physical mechanisms responsible for these outflows. BAL troughs are, by and large, not observed to be varying in velocity at a significant level (Wampler, Chugai & Petitjean 1995; Vilkoviskij & Irwin 2001; Rupke, Veilleux & Sanders 2002). However, there are several reported cases of BAL troughs varying in strength: Q1303+308 (Foltz et al. 1987), Q1413+113 (Turnshek et al. 1988), Q1246−057 (Smith & Penston 1988), UM 232 (Barlow, Junkkarinen & Burbidge 1989), QSO CSO 203 (Barlow et al. 1992), Tol 1037−270 (Srianand & Petitjean 2001), J1054+0348 (Hamann et al. 2008) FBQS J1408+3054 (Hall et al. 2011) and SDSS 1333+0012 (Vivek et al. 2012a).

Apart from these individual reports, there are six studies of BAL variability which looked for variations in a BAL QSO sample. Barlow (1994) studied a sample of 23 BAL QSOs covering time-scales of $\Delta t_{rest} \leq 1$ yr, reported optical depth variability in 15 of them and proposed the variable photo-ionizing continuum as the primary cause for these variations. Lundgren et al. (2007) analysed a sample of 29 BAL QSOs with two-epoch observations in Sloan Digital Sky Survey (SDSS) with similar time-scales and reported similar variabilities. Gibson et al. (2008) studied a sample of 13 BAL QSOs over a longer time-scale ($\Delta t_{rest} \sim 3$–6 yr). Their study found no evidence for photoionization-driven variability and indicated variations produced by changes in outflow geometry. Gibson et al. (2010), using a sample of nine BAL QSOs with multi-epoch data, reported that the scatter in the change of absorption equivalent width, ΔW, increases with the elapsed time between two epochs of

observations. Capellupo et al. (2011) studied the variability trends in the short-term (≤ 1 yr in the QSO rest frame) and long-term (≥ 1 yr in the QSO rest frame) data for a sample of 24 BAL QSOs and reported variations in 39 per cent and 65 per cent of the quasars, respectively. Capellupo et al. (2012) compared the variabilities in the C IV and Si IV lines for the above sample and found that Si IV BALs are more likely to vary than C IV BALs. Filiz Ak et al. (2012) studied the multi-epoch observations of 582 quasars in SDSS and reported 21 examples of BAL trough disappearance in 19 quasars. Very recently, Filiz Ak et al. (2013) studied the variability of 428 C IV and 235 Si IV BAL troughs identified in multi-epoch SDSS observations and reported a variability fraction of 60 per cent. In all these studies, BALs are found not to vary monotonically over time. It is also found that components at higher outflow velocities are more likely to vary than those at lower velocities, and weaker BALs are more likely to vary than stronger BALs. A co-ordinated variability between absorption lines at different velocities is interpreted as due to changing ionizing radiations whereas variability in limited portions of broad troughs are identified as movement of individual clouds across our line-of-sight. Most of the studies favour the movement of clouds across the continuum source over the changes in the ionizing continuum. The actual scenario may be a complex combination of both.

Till date, all the BAL variability studies have focused mainly on variability in C IV and Si IV lines. In this paper, we study the nature of time variability in a sample of 22 LoBAL QSOs over the redshift range $z_{em} \sim 0.3$–2.1 covering time-scales from 10 d to 7.69 years in the quasar rest frame. This work is the third paper in a series on LoBAL QSO variability. The first paper, Vivek et al. (2012a), reported the dynamical evolution of the Mg II BAL in SDSS 1333+0012. The second paper, Vivek et al. (2012b), studied the time variability of five FeLoBAL QSOs and reported for the first time significant variability in the strength of fine structure lines in the source SDSS 2215−0045. Our sample is drawn from the catalogue of BAL QSOs from the SDSS third data release (Trump et al. 2006). Typically each source has 3–5 epoch spectroscopic data. Unlike all previous studies, we supplement the spectroscopic data with long-term photometric light curves. This enables us to discuss the connection between the absorption line variability with the continuum flux variability of the QSOs.

The manuscript is arranged as follows. In Section 2, we provide details of our sample, observations and data reduction. Section 3 describes the BAL variability measurements and Section 4 gives the summary of variability in individual sources. In Section 5, we explore statistical correlations between absorption line variability and other measurable parameters from spectroscopy and photometric light curves. Discussions and summary of our results are presented in Section 6. Notes on individual variable BAL sources, Light curves and spectra of all the objects in our data are presented in the Appendix.

2 OBSERVATION AND DATA REDUCTION

Our LoBAL QSO sample consists of 22 QSOs brighter than $i = 17.5$ mag that are accessible from IUCAA Girawali Observatory (IGO). Five of these sources show broad Fe II absorption in the resonance lines and in the excited fine-structure lines.

All the new observations presented here were carried out using the 2-m telescope at IUCAA Girawali Observatory (IGO). The spectra were obtained using the IUCAA Faint Object Spectrograph (IFOSC). We have been observing the sample from the year 2006

with the aim of studying the time variability in the BALs over a range of time-scales. The detailed log of these observations together with those of the archival SDSS data and the data from the literature is given in Table 1. Basic properties of QSOs in our sample are summarized in Table 2. Spectra were obtained mainly using three grisms, Grism 1, Grism 7 and Grism 8 of IFOSC[1] in combination with 1.5 arcsec slit. These combinations cover the wavelength ranges 3270–6160 Å, 3800–6840 Å and 5800–8350 Å for the above three grisms, respectively. Fringing poses a serious issue for Grism 8 observations. We overcame this by subtracting two 2D science exposures for which the object was placed at two different locations along the slit (see Vivek et al. 2009). Typically observations were split into exposures of 45 min. All the raw frames were processed using standard IRAF[2] tasks. One-dimensional spectra were extracted from the frames using the 'DOSLIT' task in IRAF. We opted for the variance-weighted extraction as compared to the normal one. Wavelength calibrations were performed using standard helium neon lamp spectra and flux calibrations were done using a standard star spectrum observed on the same night. Air-to-vacuum conversion was applied before co-adding the spectra. Individual spectra obtained within few days were combined using $1/\sigma^2$ weighting in each pixel after scaling the overall individual spectrum to a common flux level within a sliding window. The error spectrum was computed taking into account proper error propagation during the combining process. Along with IGO data, we also used all the available spectra of the sample from SDSS data base.

We also obtained the light curves for all the sources in our sample (except for the source SDSS J0334−0711) in Johnson's *V* magnitude from the Catalina Real-Time Transient Survey (CRTS; Drake et al. 2009) to probe the variations in the ionizing continuum. The data used in these light curves are taken between 2005 April to 2010 July. More discussions on light-curve variabilities are given in Section 5.6. The light curve for all the sources is given in Figs B1–B4 in the Appendix.[3] CRTS operates with an unfiltered set up and the resulting magnitudes are converted to *V* magnitudes using the transformation equation $V = V_{ins} + a(v) + b(v)*(B − V)$, where V_{ins} is the observed open magnitude, $a(v)$ and $b(v)$ are the zero-point and the slope. The zero-point and slope are obtained from three or more comparison stars in the same field with the zero-point typically being of the order of 0.08. CRTS provides four such observations taken 10 min apart on a given night. Since we are mainly interested in the long-term variability, we have averaged these four points (or less if one or more of those coincided with bad areas) to get the light curves. We also obtained the *V* magnitudes at the SDSS epochs by convolving the SDSS spectra with Johnson's *V* band filter function. Comparison of these *V* magnitudes at SDSS epochs with the CRTS magnitudes will allow us to probe the long-term continuum flux variability.

To quantify the variations in the CRTS light curves, we carried out the following procedure. We calculated the differences in magnitudes (Δm) of all possible pairs of observations and their corresponding time differences (Δt). The median and standard deviation of the Δm values characterize the nature of variation in the sources. A larger standard deviation would imply a source where

the magnitudes have changed significantly. We then fitted a least-square minimized straight line to this Δm versus Δt data. In Fig. 1, we have plotted the Δm against the Δt and the red line marks the least-square fit. The slope of the fitted line together with the standard deviation of the Δm is used to quantify the continuum variability of the sources. Columns 8, 9 and 10 of Table 2 give the parameters of light-curve variations. Fig. 2 gives the histogram distribution of the median and standard deviation of the magnitude changes, Δm. But large photometric variations, i.e. $\sigma(\Delta m) > 0.1$ magnitudes, are seen only in three sources. These sources which exhibit large continuum variations in the CRTS light curves are SDSS J0149−0103, SDSS J1143+5203 and SDSS J2215−0045. From Figs B1 and B4 in Appendix, it is clear that in the case of J0149−0103 and J2215−0045, the light curve shows very smooth variation. In the case of J1143+5203, even though large variations are evident in the light curve, the sampling is not that good and the associated photometric errors are large. As can be seen from Fig. 1, for all sources Δm increases or decreases steadily with large time separation, except in the case of SDSS J0149−0103 and SDSS J2215−0045 where there is larger scatter in the Δm values even with in a short time period. This means that the flux in these two sources is varying appreciably even at smaller time-scales. Apart from these sources, SDSS J0318−0600, SDSS J0737+3844, SDSS J1334−0123 and SDSS J2347−1037 show larger values for the slope. As can be seen from column 10 of Table 2, the slopes are significant by more than 3σ level. Except for SDSS J0318−0600, SDSS J1143+5203 and SDSS J1334−0123, all other sources have negative slopes which means that with larger time separation, these objects tend to become fainter.

Before we proceed further, we wish to bring up a caveat in using the optical light curves to probe the ionization variability of Fe II, Mg II and Al III lines. The photons responsible for ionizing Fe^+, Mg^+ and Al^{2+} are in the far-UV range (i.e. $\lambda_{rest} < 912$ Å). Recently, Welsh, Wheatley & Neil (2011) have shown that QSOs in general show higher amplitude variability in FUV compared to NUV and optical wavelengths. Therefore, we need to be cautious while we try to correlate absorption line optical depth variability to the photometric variations seen in CRTS light curves. However, given that we have no detailed FUV light curves available for our objects, we will use the CRTS light curves keeping in mind the caveat described above.

Studies on QSO continuum light curves using structure function analysis report a monotonically increasing variability amplitude with longer time-scales e.g. (see de Vries et al. 2005). Recently, MacLeod et al. (2012) studied the optical continuum variability of SDSS QSOs with repeated observations and reported that the observed structure function is completely consistent with a damped random walk model. In their study the structure function is defined as

$$SF = 0.74 * (IQR); \quad SF_{err} = SF * 1.15/\sqrt{(N − 1)}, \quad (1)$$

where IQR is the 25–75 per cent interquartile range of the Δm distribution and N is the number of Δm values. We also looked at the continuum magnitude variations with different time-scales. Our sample spans the rest-frame wavelength range $1540 \leq \lambda_{rest} \leq 5430$ Å, redshift range $0.2 \leq z_{em} \leq 2.1$ and the luminosity range 4×10^{45} erg s$^{-1} \leq L_{Bol} \leq 4 \times 10^{47}$ erg s^{-1}. Fig. 3 shows the plot of absolute *V* band magnitude variations at different time lags. The red solid curve represents the structure function of the CRTS magnitude variability computed using equation (1). The blue dashed line shows the best fit curve to the structure function for QSO variability in the wavelength range $4000 < \lambda < 6000$ Å given by MacLeod et al. (2012). The plot

---

[1] Details of the IGO/IFOSC grisms can be found at http://www.iucaa.ernet.in/∼itp/etc/ETC/help.html#grism.

[2] IRAF is distributed by the National Optical Astronomy Observatories, which are operated by the Association of Universities for Research in Astronomy, Inc., under cooperative agreement with the National Science Foundation.

[3] Appendices B and C are available only in online version.

Table 1. Log of observations.

QSO	Instrument	Date (DD-MM-YYYY)	MJD	Exposure time (min)	λ coverage (Å)	Resolution (km s^{-1})	S/N[a]
	SDSS	23-09-2000	51812	15×6	3800–9200	150	34
	SDSS	20-11-2000	51868	15×5	3800–9200	150	34
	SDSS	01-12-2000	51879	15×4	3800–9200	150	34
J004527.68+143816.1	IGO/IFOSC 7	13-12-2007	54447	40×2	3800–6840	310	11
	IGO/IFOSC 7	18-12-2008	54818	40×2	3800–6840	310	19
	IGO/IFORS 1	22-12-2009	55187	35×3	3270–6160	370	12
	IGO/IFOSC 8	01-01-2009	54832	45×3	5800–8350	240	17
	SDSS	06-09-2000	51793	15×3	3800–9200	150	30
J014950.96−010314.1	IGO/IFOSC 7	09-01-2008	54474	45×2	3800–6840	310	11
	IGO/IFOSC 7	23-12-2008	54823	45×5	3800–6840	310	12
	SDSS	26-08-2010	55447	15×5	3800–9200	150	23
	IGO/IFOSC 7	13-02-2012	55970	45×3	3800–6840	310	11
	SDSS	29-09-2000	51816	45×1	3800–9200	150	44
J030000.57+004828.0	SDSS	29-11-2000	51877	50×1	3800–9200	150	40
(FeLoBAL QSO)	SDSS	23-10-2001	52205	45×1	3800–9200	150	33
	IGO/IFOSC 7	12-12-2007	54446	35×2	3800–6840	310	5
	IGO/IFOSC 7	27-12-2008	54817	45×8	3800–6840	310	54
	SDSS	15-01-2001	51924	80×1	3800–9200	150	27
	IGO/IFOSC 8	14-12-2007	54448	45×3	5800–8350	240	10
	IGO/IFOSC 7	09-01-2008	54474	45×3	3800–6840	310	23
J031856.62−060037.7	IGO/IFOSC 8	27-11-2008	54797	45×3	5800–8350	240	21
(FeLoBAL QSO)	IGO/IFOSC 7	31-01-2009	54862	45×4	3800–6840	310	19
	IGO/IFOSC 8	23-12-2009	55188	45×4	5800–8350	240	19
	IGO/IFOSC 7	24-12-2009	55189	45×4	3800–6840	310	17
	SDSS	01-01-2001	51910	15×3	3800–9200	150	33
J033438.28−071149.0	IGO/IFORS 1	20-01-2010	55216	45×4	3270–6160	370	28
	IGO/IFORS 1	24-01-2012	55950	45×2	3270–6160	370	7
	SDSS	29-11-2000	51877	15×3	3800–9200	150	37
	IGO/IFOSC 7	21-12-2006	54090	30×2	3800–6840	310	6
	IGO/IFOSC 7	04-12-2008	54804	45×3	3800–6840	310	29
J073739.96+384413.2	IGO/IFORS 1	24-12-2009	55189	45×3	3270–6160	370	34
	IGO/IFOSC 8	05-12-2008	54805	45×4	5800–8350	240	32
	IGO/IFOSC 8	31-01-2009	54862	45×3	5800–8350	240	34
	IGO/IFOSC 8	25-02-2009	54887	45×3	5800–8350	240	28
	SDSS	24-12-2001	52207	20×7	3800–9200	150	30
J082319.65+433433.7	SDSS	19-02-2001	51959	15×3	3800–9200	150	21
	IGO/IFORS 1	13-12-2007	54447	40×3	3270–6160	370	7
	IGO/IFOSC 7	06-12-2008	54806	45×3	3800–6840	310	20
	IGO/IFOSC 7	19-04-2009	54575	45×2	3800–6840	310	2
	IGO/IFOSC 7	25-01-2010	55221	45×3	3800–6840	310	8
	SDSS	19-11-2001	52232	48×1	3800–9200	150	26
J083522.77+424258.3	IGO/IFORS 1	14-12-2007	54448	45×3	3270–6160	370	9
(FeLoBAL QSO)	IGO/IFOSC 7	05-12-2008	54805	45×3	3800–6840	310	21
	IGO/IFOSC 7	21-01-2010	55217	45×3	3800–6840	310	29
	SDSS	15-02-2002	52320	50×1	3800–9200	150	40
J084044.41+363327.8	IGO/IFOSC 7	20-12-2006	54089	45×3	3800–6840	310	8
(FeLoBAL QSO)	IGO/IFOSC 7	12-12-2007	54446	45×3	3800–6840	310	23
	IGO/IFOSC 7	07-12-2008	54807	45×4	3800–6840	310	26
	IGO/IFOSC 7	17-12-2009	55182	45×6	3800–6840	310	50
	SDSS	27-11-2002	52605	15×6	3800–9200	150	34
J085053.12+445122.4	IGO/IFORS 1	19-01-2010	55215	45×5	3270–6160	370	31
	IGO/IFORS 1	12-03-2011	55632	45×5	3270–6160	370	16
	SDSS	12-03-2003	52710	15×3	3800–9200	150	45
J094443.13+062507.4	IGO/IFOSC 7	03-04-2008	54559	40×3	3800–6840	310	45
	IGO/IFOSC 7	30-01-2009	54861	45×5	3800–6840	310	60

Table 1 – *continued*

QSO	Instrument	Date (DD-MM-YYYY)	MJD	Exposure time (mins)	λ coverage (Å)	Resolution (km s^{-1})	S/N^a
	IGO/IFOSC 7	24-01-2010	55220	45×2	3800–6840	310	28
J094443.13+062507.4	IGO/IFOSC 7	11-04-2010	55297	45×2	3800–6840	310	20
	IGO/IFOSC 7	14-03-2011	55634	45×4	3800–6840	310	50
	SDSS	30-12-2000	51908	15×3	3800–9200	150	27
	IGO/IFOSC 7	03-04-2008	54559	40×3	3800–6840	310	22
J095232.21+025728.3	IGO/IFOSC 7	25-02-2009	54887	45×3	3800–6840	310	25
	IGO/IFOSC 7	25-01-2010	55221	45×3	3800–6840	310	10
	IGO/IFOSC 7	15-03-2011	55635	45×5	3800–6840	310	19
	SDSS	12-04-2002	52376	15×3	3800–9200	150	23
J101053.98+451817.0	IGO/IFORS 1	09-01-2008	54474	45×3	3270–6160	370	14
	IGO/IFORS 1	26-02-2009	54888	45×3	3270–6160	370	17
	IGO/IFORS 1	24-01-2010	55220	45×4	3270–6160	370	18
	SDSS	03-01-2003	52642	15×3	3800–9200	150	24
J112822.42+482310.0	IGO/IFOSC 7	22-01-2010	55218	45×3	3800–6840	310	23
	IGO/IFOSC 7	14-03-2011	55634	45×4	3800–6840	310	22
	SDSS	04-04-2002	52368	15×3	3800–9200	150	25
J114340.96+520303.3	IGO/IFORS 1	08-01-2008	54473	40×2	3270–6160	370	11
	IGO/IFORS 1	28-01-2009	54859	45×2	3270–6160	370	13
	SDSS	25-04-2001	52024	15×6	3800–9200	150	62
J120813.42+023015.1	IGO/IFOSC 7	23-01-2010	55219	40×3	3800–6840	310	57
	IGO/IFOSC 7	13-03-2011	55633	45×3	3800–6840	310	42
	SDSS	28-04-2000	51662	15×3	3800–9200	150	27
	SDSS	15-02-2001	51955	15×7	3800–9200	150	40
	IGO/IFOSC 7	03-04-2008	54559	40×2	3800–6840	300	11
J133356.02+001229.1	IGO/IFORS 1	26-02-2009	54888	45×3	3270–6160	360	21
	IGO/IFOSC 7	26-03-2009	54916	45×5	3800–6840	300	15
	IGO/IFORS 1	22-01-2010	55218	45×5	3270–6160	360	26
	IGO/IFOSC 7	06-04-2011	55657	45×3	3800–6840	300	19
	SDSS	01-06-2002	52426	15×3	3800–9200	150	30
J133428.06−012349.0	IGO/IFOSC 7	04-04-2008	54560	40×3	3800–6840	310	18
	IGO/IFOSC 7	23-12-2008	54823	45×5	3800–6840	310	30
	SDSS	21-04-2001	52026	15×8	3800–9200	150	53
J144842.45+042403.1	IGO/IFORS 1	01-04-2010	55287	45×2	3270–6160	370	9
	IGO/IFOSC 8	22-03-2010	55277	45×2	5800–8350	240	12
	IGO/IFOSC 7	15-03-2011	55635	45×3	3800–6840	310	22
	SDSS	05-05-2003	52764	15×3	3800–9200	150	33
J161425.17+375210.7	IGO/IFOSC 7	03-04-2008	54559	40×1	3800–6840	310	19
	IGO/IFOSC 7	11-04-2010	55297	45×3	3800–6840	310	25
	IGO/IFOSC 7	07-04-2011	55658	45×1	3800–6840	310	27
	SDSS	04-09-2000	51804	53×1	3800–9200	150	41
	VLT/FORS1	20-09-2003	52902	5×1	3300–11000	370	62
J221511.93-004550.0	IGO/IFOSC 7	31-10-2008	54783	45×4	3800–6840	310	38
(FeLoBAL QSO)	IGO/IFOSC 8	01-11-2008	54784	45×4	5800–8350	240	39
	IGO/IFORS 1	04-01-2010	55213	45×8	3270–6160	370	9
	MagE	10-08-2010	55431	15×1	3100–10000	70	16
	SDSS	12-10-2002	52559	15×3	3800–9200	150	28
	SDSS	19-08-2007	54331	15×5	3800–9200	150	38
J234711.44-103742.4	IGO/IFOSC 7	31-10-2008	54770	45×3	3800–6840	310	19
	IGO/IFOSC 8	21-11-2008	54791	45×4	5800–8350	240	19
	IGO/IFOSC 7	15-12-2009	55180	35×2	3800–6840	310	8

^{a}The values quoted are mean of S/N calculated per pixel over the wavelength range 5800 Å–6200 Å.

Table 2. Source parameters measured from the data.

Name (1)	z_{em} (2)	z_{abs} (3)	V_{max} (km s^{-1}) (4)	$\langle w \rangle$ (Å) (5)	L_{Bol} (erg s^{-1}) (6)	M_{BH} (M$_\odot$) (7)	Δm (mag) (8)	$\sigma(\Delta m)$ (mag) (9)	Slope($\Delta m/\Delta t$) (mag yr^{-1}) (10)	Abs. line(s) probed (11)
J0045+1438	1.992	1.948	5746.5	6.93	3.9×10^{47}	3.2E+09	-0.04	0.04	-0.032 ± 0.007	Al III
J0149−0103‡	1.074	1.030	7910.7	5.60	8.4×10^{46}	6.8E+08	-0.01	0.13	-0.046 ± 0.007	Mg II
J0300+0048†	0.568	0.864	6492.8	–	3.8×10^{45}	3.0E+07	0.01	0.04	-0.003 ± 0.024	Mg II
J0318−0600†	1.968	1.941	7612.2	14.57	7.3×10^{46}	5.9E+08	0.07	0.05	0.075 ± 0.021	Mg II,Al III
J0334−0711	0.634	0.600	7537.6	6.50	4.3×10^{46}	3.5E+08	–	–	–	Mg II
J0737+3844‡	1.400	1.374	5000.2	7.16	1.8×10^{47}	1.5E+09	-0.07	0.06	-0.068 ± 0.004	Mg II,Al III
J0823+4334	1.660	1.620	11045.0	5.44^a	2.2×10^{47}	1.8E+09	-0.03	0.04	-0.036 ± 0.009	Al III
J0835+4242†	0.810	0.769	1865.9	4.96	3.9×10^{46}	3.2E+08	-0.04	0.07	-0.005 ± 0.008	Mg II
J0840+3633†	1.230	1.225	3880.8	32.13	8.1×10^{45}	6.6E+07	0.03	0.04	0.015 ± 0.008	Mg II,Al III
J0850+4451	0.541	0.524	5224.1	17.22	2.1×10^{46}	1.7E+08	0.01	0.05	0.014 ± 0.006	Mg II
J0944+0625‡	0.695	0.653	8507.7	15.55	1.3×10^{47}	1.0E+09	0.04	0.04	0.010 ± 0.004	Mg II
J0952+0257	1.355	1.301	18209.2	16.99	1.5×10^{47}	1.2E+09	0.03	0.06	-0.002 ± 0.007	Mg II,Al III
J1010+4518‡	1.776	1.705	12910.7	7.21^a	1.6×10^{47}	1.3E+09	-0.02	0.07	-0.014 ± 0.012	Al III
J1128+4823	0.543	0.536	5895.8	11.82	1.5×10^{46}	1.2E+08	-0.01	0.06	0.010 ± 0.009	Mg II
J1143+5203‡	1.816	1.788	18209.2	11.64^a	2.9×10^{47}	2.3E+09	0.06	0.11	0.041 ± 0.016	Al III
J1208+0230‡	1.180	1.067	17836.1	4.37	3.8×10^{47}	3.1E+09	-0.04	0.03	-0.032 ± 0.004	Mg II
J1333+0012	0.918	0.811	20746.5	7.04	9.4×10^{46}	7.6E+08	0.06	0.08	0.008 ± 0.005	Mg II
J1334−0123‡	1.876	1.833	18507.7	23.66^a	2.6×10^{47}	2.1E+09	0.07	0.06	0.058 ± 0.012	Mg II,Al III
J1448+0424	1.546	1.516	5821.1	8.02	3.8×10^{47}	3.1E+09	-0.01	0.03	-0.012 ± 0.010	Mg II,Al III
J1614+3752	0.553	0.525	6492.8	3.43	3.8×10^{46}	3.1E+08	-0.04	0.08	-0.026 ± 0.004	Mg II
J2215−0045†‡	1.478	1.360	18582.3	21.76	2.8×10^{47}	2.3E+09	-0.01	0.19	-0.123 ± 0.009	Mg II,Al III
J2347−1037	1.800	1.711	15522.6	27.46	2.6×10^{47}	2.1E+09	-0.07	0.06	-0.072 ± 0.008	Al III

Notes. Col. 1: QSO name, †FeLoBAL QSO sources, ‡Sources with strong Fe emission; Col. 2: z_{em} is obtained from the fitting of SDSS composite; Col. 3: z_{abs} corresponds to the maximum optical depth; Col. 4: V_{max} is calculated for the Mg II line from the normalized SDSS spectra. V_{max} is identified as the maximum velocity at which source flux matches with the continuum; Col. 5: average Mg II equivalent widths, ^{a}corresponds to average Al III equivalent widths; Col. 6: L_{Bol} is computed using the prescription, $L_{Bol} = 7.9 \times \nu F_{\nu B}$, of Marconi et al. (2004); Col. 7: M_{BH} is derived from L_{Bol} assuming Eddington accretion; Col. 8: median Δm values; Col. 9: standard deviation of Δm values; Col. 10: slope of $\Delta m - \Delta t$ graph; Col. 11: absorption line(s) probed in this study.

clearly agrees with the already known result of larger variations at larger time lags. But, the sources in our sample are less variable at shorter time lags as compared to the non-BAL QSOs. This could be related to the fact that we picked up bright LoBAL QSOs for our spectroscopic monitoring and bright QSOs tend to vary less and on longer time-scales.

3 BAL VARIABILITY MEASUREMENTS

We define two metrics to quantify the absorption line variability. First one is the variation in the equivalent width between different epochs. Equivalent widths are computed by normalizing the spectra using a spectral energy distribution (SED) in the optical-UV region, obtained by fitting the absorption/emission free regions with a template spectrum (see below). Optical-UV SED is obtained by fitting the observed spectrum $f(\lambda)$ with the template spectrum $f_t(\lambda)$ using the following parametrization,

$$f(\lambda) = \left[af_t(\lambda) + b \left(\frac{\lambda}{\lambda_0} \right)^\alpha \right] e^{-\tau_\lambda}. \qquad (2)$$

We use the χ^2-minimization to get the best values for parameters a, b, α and τ_λ. The second term in the above equation denotes the spectral index differences between the observed and the template QSO spectra. The dust optical depth τ_λ is obtained assuming a Small Magellanic Cloud (SMC) like extinction curve. The fitting method is similar to that described by Srianand et al. (2008). In the case of strong Fe emitters, we use the spectrum of a strong Fe emitting source SDSS 0923+5745 as the template (see Vivek et al. 2012b).

In all other but two cases, we use the SDSS composite spectrum as the template (Richards et al. 2002). For SDSS J0045+1438 and SDSS J2347−1037, the fitting did not converge to a good fit. So, we used a simple polynomial connecting line free regions to approximate the continuum. The computed equivalent widths are given in Table 4.

Equivalent width measurements are sensitive to the correct estimation of the continuum. In the case of BAL quasars, continuum measurements are difficult as the spectra are dominated by BALs. We define the second metric, integrated ratio, to avoid the ambiguities in the continuum. The ratio spectra for all the epochs with respect to a reference epoch (first epoch) are integrated over the wavelength range covered by the BAL absorption to get the integrated ratio values. The computed integrated ratio values between different epoch spectra are given in Table 5.

In one source, SDSS J0300+0048, the continuum is completely dominated by absorption lines. Hence, we did not compute the equivalent widths and integrated ratios in this case. But, it can be seen from fig. 2 of Vivek et al. (2012b) that this source does not show any variation in Mg II absorption. Hence, we include this source as a non-varying one in our analysis. Equivalent widths and integrated ratios were measured for the rest of the sample.

We identified sources showing absorption line variability as those having more than 3σ variations in the equivalent widths and 5σ in the integrated ratio values between any two epochs. As the equivalent width measurements are prone to uncertainties related to continuum placements, we do not include those sources which have equivalent width variations, but show no significant changes in ratios.
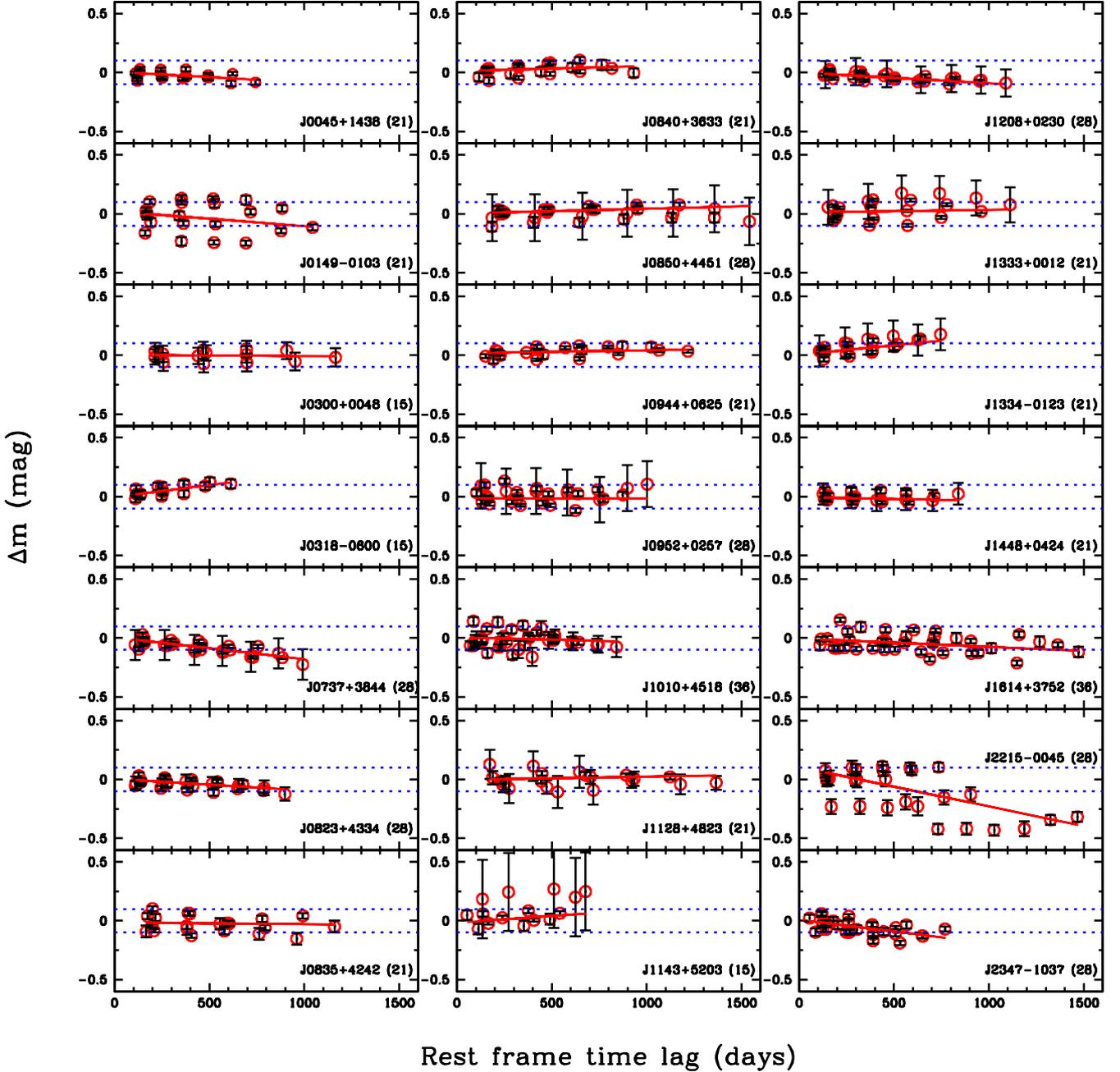
Figure 1. Results of long-term photometric monitoring of sources in our sample from CRTS. The *x*-axis represents rest-frame pairwise time lags and the *y*-axis represents pairwise magnitude differences for each source measured over different time lags. The red/grey line marks the least-square fit to the data. The number in parenthesis indicates the number of independent photometric measurements available for the source. Blue dotted horizontal lines correspond to magnitude variations of 0.1 mag. We consider those objects as variable for which $\sigma(\Delta m) > 0.1$ mag. Variations above this value are seen in the case of SDSS J0149−0103 and SDSS J2215−0045. In the case of SDSS J1143+5203, large photometric variations are seen albeit large photometric errors.

4 SUMMARY OF VARIABILITY IN INDIVIDUAL SOURCES

Detailed distribution of individual sources showing absorption line variations is given in the Appendix.

We detect BAL variability in eight sources in our sample of 22 QSOs. All these sources show equivalent width variations at $>3\sigma$ level and the ratio variations at $>5\sigma$ level. The summary of the comparison between the equivalent width and continuum flux variations over long and short time-scales is given in Table 3. Fig. 4

shows the comparison of spectra showing maximum absorption line changes for six sources in our sample. Similar plots for the remaining sources, SDSS J1333+0012 and SDSS J2215−0045, are already published in Vivek et al. (2012a,b), respectively.

Four sources, SDSS J0045+1438, SDSS J0149−0103, SDSS J0944+0625 and SDSS J1333+0012, show absorption line variations at both short (<1 year) and long (>1 year) time-scales. Except in the case of SDSS J0045+1438, where the variations are seen in Al III BAL, the remaining three sources show variations in the Mg II
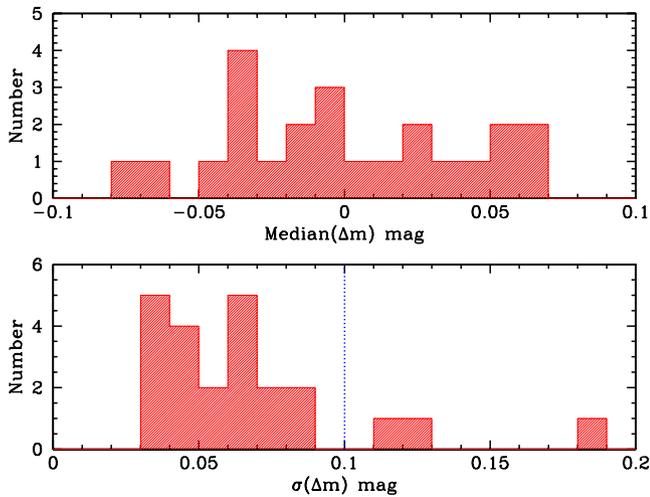
Figure 2. Histogram of the median magnitude differences (top panel) and the standard deviation of the magnitude differences Δm (bottom panel) for each source. Blue/dotted vertical line corresponds to $\sigma(\Delta m) \sim 0.1$. Large photometric variations (~ 0.1 mag) are only seen in three sources, SDSS J0149−0103, SDSS J1143+5203, and SDSS J2215−0045. However, in the case of SDSS J1143+5203, the photometric errors are also large (see Fig. 1).
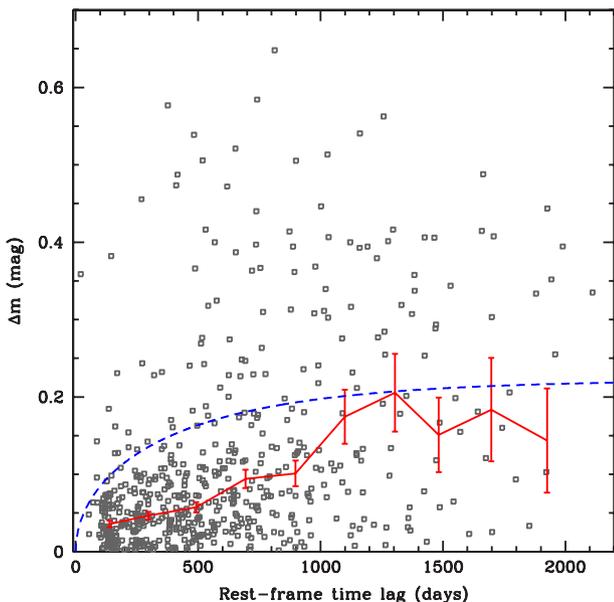

Figure 3. Plot of Δm versus rest-frame time lags. Grey points represent the pairwise magnitude differences measured over different time lags. The red solid curve represents the structure function (in mag) of the CRTS magnitude variations of LoBAL QSOs in our sample. The blue dashed line shows the best-fitting curve to the structure function for SDSS quasars in the wavelength range $4000 < \lambda < 6000$ Å given by MacLeod et al. (2012). Clearly, the variability increases over larger time lags. But, sources in our sample are more luminous and have smaller variability at smaller time-scales as compared to SDSS quasars.

line. In two cases, SDSS J0149−0103 and SDSS J1333+0012, the profile variations are consistent with dynamical changes like movement of clouds across the line of sight causing the absorption line variations. In the case of SDSS J0045+1438, Al III variation occurs without appreciable change in the continuum whereas coherent variations are seen in both continuum and absorption lines for the other three sources. The role of ionization-induced variability cannot be

dismissed in these three cases. We note that the shape of the light curves for these continuum varying sources has a curvature (see Appendix B).

The remaining four sources, SDSS J0850+4451, SDSS J0952+0257, SDSS J1208+0230 and SDSS J2215−0045, show only long-term absorption line variations. The observed variations in SDSS J1208+0230 and SDSS J2215−0045 are again consistent with the dynamical changes in the clouds (Vivek et al. 2012b). Among these four sources, only SDSS J2215−0045 has shown significant coherent changes in the continuum light curve.

Moreover, we also identify three sources, SDSS J0318−0600, SDSS J0737+3844 and SDSS J2347−1037, where coherent variations with more than 0.1 mag are seen in the CRTS light curves (with a significant slope in $\Delta m - \Delta t$ plot; see Fig. 2) without any absorption line variations (see Fig. B1). Overall, both the absorption lines and continuum have varied in several sources in the sample. But, there are enough indications to suggest that the two variations need not be related. We check this in the next section.

5 STATISTICAL ANALYSIS OF THE VARIABILITY OF LOBAL QSOS

In this section, we study the correlations between absorption line variability and other properties of low ionization BAL QSOs. For this purpose, we divide the sample into several sub-groups.

5.1 Absorption line variability in different groups of LoBAL QSOs

The fraction of varying BALs in our overall sample is small (i.e. 36 per cent) as compared to C IV BALs from previous studies. Capellupo et al. (2011) used a slightly higher threshold (4σ) to define the variability. In our sample, only one source shows variations less than 4σ. A higher threshold will again reduce the fraction of variable sources in our sample. There are eight BAL QSOs with emission redshift $0.5 < z_{em} < 1.2$ where only Mg II absorption lines are covered. Based on the absence of Fe II absorption, we confirm that these are not FeLoBAL QSOs. However, the presence of Al III absorption cannot be confirmed as we do not cover the expected wavelength range of Al III absorption lines. Five out of these eight systems (i.e. 63 per cent) show optical depth variation. This fraction becomes 50 per cent if we include the two low-redshift FeLoBAL QSOs. Among these five, three systems show only long-term absorption line variability. In the remaining systems, absorption line variability is seen over all time-scales.

There are 12 sources that show detectable Mg II and Al III absorption. They typically have redshift greater than 1.2. Out of these, three are FeLoBAL QSOs. SDSS J2215−0045 is the only FeLoBAL QSO source which shows variations in Mg II and Al III lines. Only in four sources, SDSS J0737+3844, SDSS J0952+0257, SDSS J1334−0123 and SDSS J1448+0424, both Mg II and Al III lines are simultaneously covered. In the remaining sources, we use only the Al III to study the absorption line variability. Out of the nine non-FeLoBAL QSOs in this sub-sample, two (i.e. 22 per cent) show variations in the optical depth. The percentage of sources with variable BALs slightly increases to 25 per cent (3/12) when FeLoBAL QSOs are also included. These results suggest that Mg II BAL QSOs at $z_{em} < 1.2$ seem to show larger variability compared to high-redshift Mg II BAL QSOs. We notice that the luminosity distribution of the two samples is nearly identical. However, the longest monitoring time-scale (in the QSO's rest frame) is roughly

Table 3. Summary of the variation in equivalent width and continuum flux. Rest-frame variations occurring within a year are termed as short time-scale. The arrow indicates the direction of variation. $\uparrow$ indicates a positive change (more absorption) and $\downarrow$ indicates a negative change (less absorption).

Name	Location of absorption changes (km s^{-1})	Rest-frame variations detected?			
		Equivalent width		Continuum flux	
		Long time-scale	Short time-scale	Long time-scale	Short time-scale
J0045+1438	-3650	Yes $\downarrow$	Yes $\downarrow$	Yes $\uparrow$	No
J0149$-$0103	-7100	Yes $\uparrow$	Yes $\downarrow$	Yes $\uparrow$	Yes $\uparrow$
J0850+4451	-3490	Yes $\uparrow$	No	Yes $\downarrow$	No
J0944+0625	-7300	Yes $\downarrow$	Yes $\downarrow$	Yes $\uparrow$	Yes $\downarrow$
J0952+0257	-8500	Yes $\downarrow$	No	Yes $\uparrow$	Yes $\uparrow\downarrow$
J1208+0230	-15100	Yes $\downarrow$	No	Yes $\uparrow$	No
J1333+0012	-25500	Yes $\downarrow\uparrow$[a]	Yes $\uparrow\downarrow$	Yes $\downarrow$	Yes $\uparrow$
J2215$-$0045	-13500	Yes $\downarrow$	No	Yes $\uparrow$	No

[a]One component increased and another component decreased.

Table 4. Equivalent width measurements.

Name	Ion	Epoch ID	MJD	λ range (Å)	$W_{\rm rest}$ (Å)	Comments
	Mg II	sdss1	51810		7.0 ± 0.3	
	Mg II	sdss2	51868	7911.9–8280.8	7.6 ± 0.3	
	Mg II	sdss3	51879		6.3 ± 0.3	
	Al III	sdss1	51810		3.5 ± 0.1	
	Al III	sdss2	51868		3.3 ± 0.1	
	Al III	sdss3	51879	5439.9–5514.1	3.1 ± 0.1	
SDSS J0045+1438	Al III	2007	54447		3.0 ± 0.3	Variable
	Al III	2008	54818		2.8 ± 0.2	
	Al III	2009	55187		1.9 ± 0.3	
	C IV	sdss1	51810		53.7 ± 0.2	
	C IV	sdss2	51868		55.2 ± 0.3	
	C IV	sdss3	51879	4378.2–4579.6	54.2 ± 0.2	
	C IV	2007	54447		47.9 ± 0.8	
	C IV	2008	54818		50.1 ± 0.4	
	C IV	2009	55187		48.3 ± 0.6	
	Mg II	sdss	51793		5.3 ± 0.2	
SDSS J0149$-$0103	Mg II	2008	54474	5642.1–5722.3	6.1 ± 0.5	Variable
	Mg II	2009	54823		6.3 ± 0.2	
	Mg II	2010	55447		5.8 ± 0.1	
	Mg II	2012	55970		4.7 ± 0.4	
	Mg II	sdss	51924		14.8 ± 0.1	
	Mg II	2007	54448		14.6 ± 0.2	
SDSS J0318$-$0600	Mg II	2008	54797	8087.3–8250.7	14.5 ± 0.1	
	Mg II	2009	55188		14.6 ± 0.1	
	Mg II	sdss	51910		6.7 ± 0.1	
SDSS J0334$-$0711	Mg II	2010	55216	4458.5–4486.1	6.6 ± 0.1	
	Mg II	2012	55950		6.2 ± 0.3	
	Mg II	sdss	51877		7.3 ± 0.1	
	Mg II	2006	54090		6.9 ± 0.6	
	Mg II	2008	54804	6609.2–6676.4	7.0 ± 0.2	
	Mg II	2009	55189		7.3 ± 0.1	
SDSS J0737+3844	Mg II	2010	54887		7.4 ± 0.1	
	Al III	sdss	51877		5.8 ± 0.2	
	Al III	2006	54090		3.6 ± 1.2	
	Al III	2008	54804	4374.4–4442.0	6.3 ± 0.3	
	Al III	2009	54887		5.9 ± 0.1	
	Al III	sdss1	52207		5.7 ± 0.1	
	Al III	sdss2	51959		5.0 ± 0.3	
SDSS J0823+4334	Al III	2007	54447	4779.1–4901.4	6.5 ± 0.7	
	Al III	2008	54806		5.1 ± 0.3	

Table 4 – *continued*

Name	Ion	Epoch ID	MJD	λ range (Å)	W_{rest} (Å)	Comments
	Al III	2009	54940		4.7 ± 2.2	
	Al III	2010	55221		5.7 ± 0.7	
	Mg II	sdss	52232		4.4 ± 0.2	
SDSS J0835+4242	Mg II	2007	54448		4.8 ± 0.3	
	Mg II	2008	54805	5027.7–5066.5	4.8 ± 0.3	
	Mg II	2010	55217		5.9 ± 0.2	
	Mg II	sdss	52320		32.1 ± 0.1	
	Mg II	2006	54089		31.8 ± 0.2	
SDSS J0840+3633	Mg II	2007	54446	6158.3–6242.5	32.0 ± 0.1	
	Mg II	2008	54807		32.5 ± 0.1	
	Mg II	2009	55182		32.2 ± 0.1	
	Mg II	sdss	52605		12.6 ± 0.4	
SDSS J0850+4451	Mg II	2010	55215	4225.3–4294.0	19.1 ± 0.3	Variable
	Mg II	2011	55632		18.3 ± 0.5	
	Mg II	2012	56044		18.9 ± 0.6	
	Mg II	sdss	52710		17.6 ± 0.1	
	Mg II	2008	54559		16.5 ± 0.1	
SDSS J0944+0625	Mg II	2009	54861	4603.1–4694.7	16.0 ± 0.1	Variable
	Mg II	2010	55220		14.2 ± 0.2	
	Mg II	2010	55297		14.5 ± 0.2	
	Mg II	2011	55634		14.6 ± 0.1	
	Mg II	sdss	51908		18.6 ± 0.3	
	Mg II	2008	54559		16.8 ± 0.3	
	Mg II	2009	54887	6279.1–6464.1	16.9 ± 0.3	
	Mg II	2010	55221		16.2 ± 0.6	
	Mg II	2011	55635		16.5 ± 0.3	
SDSS J0952+0257	Al III	sdss	51908		9.6 ± 0.2	
	Al III	2008	54559		7.4 ± 0.3	Variable
	Al III	2009	54887	4211.9–4293.1	8.2 ± 0.2	
	Al III	2010	55221		6.4 ± 0.8	
	Al III	2011	55635		8.4 ± 0.3	
	Al III	sdss	52376		7.1 ± 0.2	
SDSS J1010+4518	Al III	2008	54474	4939.1–5061.4	7.8 ± 0.4	
	Al III	2009	54888		7.0 ± 0.3	
	Al III	2010	55220		7.1 ± 0.3	
	Mg II	sdss	52642		13.5 ± 0.3	
SDSS J1128+4823	Mg II	2010	55218	4228.9–4330.4	9.3 ± 0.4	
	Mg II	2011	55634		12.6 ± 0.4	
	Al III	sdss	52368		12.9 ± 0.3	
SDSS J1143+5203	Al III	2008	54473	7770.1–7848.9	12.1 ± 0.6	
	Al III	2009	54859		12.2 ± 0.5	
	Mg II	sdss	52024		5.6 ± 0.2	
SDSS J1208+0230	Mg II	2010	55219	5743.2–5813.1	4.1 ± 0.2	Variable
	Mg II	2011	55633		3.4 ± 0.2	
	Mg II	sdss1	51662		2.5 ± 0.2	
	Mg II	sdss2	51955		2.8 ± 0.1	
	Mg II	2008	54559		0.1 ± 0.4	
SDSS J1333+0012	Mg II	2009(7)†	54888	5035.7–5090.9	0.3 ± 0.3	Variable
R component	Mg II	2009(1)†	54916		0.3 ± 0.2	
	Mg II	2010	55218		0.4 ± 0.1	
	Mg II	2011	55657		0.7 ± 0.2	
	Mg II	sdss1	51662		0.2 ± 0.3	
	Mg II	sdss2	51955		4.4 ± 0.2	
	Mg II	2008	54559		6.3 ± 0.7	
SDSS J1333+0012	Mg II	2009(7)†	54888	4790.7–5000.9	12.0 ± 0.5	Variable

Table 4 – *continued*

Name	Ion	Epoch ID	MJD	λ range (Å)	W_{rest} (Å)	Comments
B component	Mg II	2009(1)†	54916		14.1 ± 0.3	
	Mg II	2010	55218		7.1 ± 0.2	
	Mg II	2011	55657		5.1 ± 0.4	
	Al III	sdss1	52426		24.5 ± 0.1	
SDSS J1334−0123	Al III	2008	54560	5142.5–5302.9	23.6 ± 0.2	
	Al III	2009	54823		23.6 ± 0.1	
	Al III	sdss2	55272		23.0 ± 0.4	
	Mg II	sdss1	52026		7.8 ± 0.1	
	Mg II	sdss2	55706		7.9 ± 0.1	
	Mg II	2010	55287	6979.6–7064.4	8.4 ± 0.2	
SDSS J1448+0424	Mg II	2011	55635		7.9 ± 0.1	
	Al III	sdss1	52026		5.7 ± 0.1	
	Al III	sdss2	55706		5.9 ± 0.1	
	Al III	2010	55287	4624.1–4698.8	5.5 ± 0.4	
	Al III	2011	55635		5.4 ± 0.2	
	Mg II	sdss	52764		4.0 ± 0.1	
SDSS J1614+3752	Mg II	2008	54559	4250.4–4301.4	3.3 ± 0.4	
	Mg II	2010	55297		3.3 ± 0.3	
	Mg II	2011	55658		3.1 ± 0.3	
	Mg II	sdss	51804		25.8 ± 0.2	
	Mg II	vlt	52902		22.4 ± 0.2	
SDSS J2215−0045	Mg II	2008	54783	6512.2–6735.2	19.2 ± 0.2	Variable
	Mg II	mage	55431		20.6 ± 0.2	
	Mg II	2011	55545		20.8 ± 0.4	
	Al III	sdss	51804		3.9 ± 0.1	
	Al III	vlt	52902		2.6 ± 0.1	
	Al III	2008	54783	4345.0–4419.6	1.1 ± 0.1	
	Al III	2010	55213		1.1 ± 0.3	
	Al III	mage	55431		1.0 ± 0.1	
	Al III	2011	55545		1.1 ± 0.1	
	Mg II	sdss1	52559	7448.6–7716.4	27.4 ± 0.3	
	Mg II	sdss2	54331		27.5 ± 0.2	
SDSS J2347−1037	Al III	sdss1	52559		20.2 ± 0.1	
	Al III	sdss2	54331		20.0 ± 0.1	
	Al III	2008	54770	4932.0–5110.4	20.4 ± 0.3	
	Al III	2009	55180		21.3 ± 0.7	

†7 and 1 in the parenthesis refer to IFOSC 7 and IFORS 1 data, respectively.

60 per cent less for the high-z sub-sample. Moreover, the median long-term variability time-scale (∼1200 d) is close to the maximum time-scale probed in some of the high-z QSOs. Therefore, further spectroscopic monitoring of these sources is needed to confirm the apparent excess variability seen in low-z BAL QSOs.

Next we consider a sub-sample of FeLoBAL QSOs. Full details of this sub-sample is published in Vivek et al. (2012b). Only one out of five sources (i.e. 20 per cent) considered in this study has shown significant absorption line variability. The fraction of FeLoBAL QSO systems showing absorption line variations (i.e. 20 per cent) is less than that seen for the Mg II BALs without Fe II (i.e. 41 per cent). There are indications, in cases where independent constraints on ionization parameter and density can be obtained, that the FeLoBAL QSOs may originate far away (i.e. >1 kpc) from the central engine (see Korista et al. 2008; Moe et al. 2009; Dunn et al. 2010; Bautista et al. 2010; Faucher-Giguère, Quataert & Murray 2012). Based on optical-IR observations Farrah et al. (2007) suggested that FeLoBAL QSOs depict an evolutionary phase in which a luminous starburst phase in a galaxy is approaching its end stage

and the QSO phase is beginning. It is also proposed that the observed properties of FeLoBAL QSOs are readily explained if they are formed in situ in the dense ISM shock heated by QSO blast waves (Faucher-Giguère et al. 2012). Our study favours FeLoBAL QSOs to have a different origin compared to LoBAL QSOs. If one can associate rapid absorption line variability to gas close to the QSOs, then our results either favour FeLoBAL QSOs originate from a larger distance to the central engine or from a time-steady flow as compared to LoBAL QSOs without Fe absorption. However, Lazarova et al. (2012) do not find differences in the FIR properties of LoBAL and non-LoBAL QSOs. Note that both the results mentioned above are based on small number statistics. It will be good to probe the exact nature of LoBAL QSOs with a larger sample.

There are eight sources in the sample which have optical-UV SEDs dominated by strong Fe emission lines. These sources have a broad Fe emission feature mimicking an absorption slightly blueward of the Mg II emission line. Some of the variations in Mg II lines can be attributed to the variation in this Fe emission feature. Therefore, we did not include wavelengths covering this feature in

Table 5. Variability based on ratio between two epochs.

Name	Ion	Epoch ID 1	Epoch ID 2	λ range (Å)	Ratio	Comments
	Mg II	sdss1	sdss2		2.9 ± 1.4	
	Mg II	sdss1	sdss3	7911.9–8280.8	−2.2 ± 1.3	
	Al III	sdss1	sdss2		−1.0 ± 0.5	
	Al III	sdss1	sdss3		0.4 ± 0.5	
	Al III	sdss1	2007	5439.9–5514.1	−5.9 ± 1.1	
SDSS J0045+1438	Al III	sdss1	2008		−4.8 ± 0.7	Variable
	Al III	sdss1	2009		−3.4 ± 0.9	
	C IV	sdss1	sdss2		1.2 ± 2.8	
	C IV	sdss1	sdss3		5.6 ± 2.7	
	C IV	sdss1	2007	4378.2–4579.6	−26.4 ± 5.8	
	C IV	sdss1	2008		−19.3 ± 3.6	
	C IV	sdss1	2009		−47.9 ± 4.9	
	Mg II	2008	2009		−1.1 ± 1.3	
	Mg II	2008	2012		−7.6 ± 1.5	
	Mg II	2009	2008		0.7 ± 1.2	
SDSS J0149−0103	Mg II	2009	2012	5642.1–5722.3	−8.4 ± 1.2	Variable
	Mg II	sdss	2008		4.6 ± 1.1	
	Mg II	sdss	2009		4.5 ± 1.0	
	Mg II	sdss	2010		3.1 ± 0.5	
	Mg II	sdss	2012		−2.0 ± 1.0	
	Mg II	sdss	2007		1.7 ± 1.6	
SDSS J0318−0600	Mg II	sdss	2008	8087.3–8250.7	1.3 ± 0.6	
	Mg II	sdss	2009		1.9 ± 0.8	
	Mg II	sdss	2010		−1.4 ± 0.3	
SDSS J0334−0711	Mg II	sdss	2012	4458.5–4486.1	−1.6 ± 0.9	
	Mg II	2010	2012		−0.3 ± 1.0	
	Mg II	sdss	2006		2.9 ± 2.0	
	Mg II	sdss	2008		−0.4 ± 0.5	
	Mg II	sdss	2009	6609.2–6676.4	−0.0 ± 0.4	
SDSS J0737+3844	Mg II	sdss	2010		−0.1 ± 0.4	
	Al III	sdss	2006		1.1 ± 2.5	
	Al III	sdss	2008	4374.4–4442.0	−1.8 ± 0.7	
	Al III	sdss	2010		−2.8 ± 0.5	
	Al III	sdss1	sdss2		−0.9 ± 0.8	
	Al III	sdss1	2007		1.6 ± 2.0	
SDSS J0823+4334	Al III	sdss1	2008	4779.1–4901.4	−2.2 ± 1.0	
	Al III	sdss1	2009		−1.5 ± 5.5	
	Al III	sdss1	2010		−1.6 ± 2.0	
	Mg II	sdss	2007		2.6 ± 0.8	
SDSS J0835+4242	Mg II	sdss	2008	5027.7–5066.5	2.9 ± 0.6	
	Mg II	sdss	2010		6.9 ± 0.4	
	Mg II	sdss	2006		−5.2 ± 5.2	
	Mg II	sdss	2007		−5.1 ± 2.7	
SDSS J0840+3633	Mg II	sdss	2008	6158.3–6242.5	−4.7 ± 1.9	
	Mg II	sdss	2009		−3.9 ± 1.4	
	Mg II	sdss	2010		4.3 ± 0.4	
	Mg II	sdss	2011		4.2 ± 0.6	
SDSS J0850+4451	Mg II	sdss	2012	4225.3–4294.0	4.5 ± 0.7	Variable
	Mg II	2010	2011		0.8 ± 0.6	
	Mg II	2010	2012		−0.2 ± 0.8	
	Mg II	2011	2012		0.5 ± 0.9	
	Mg II	sdss	2008		−2.8 ± 0.4	
	Mg II	sdss	2009		−3.1 ± 0.3	
SDSS J0944+0625	Mg II	sdss	2010	4603.1–4694.7	−9.8 ± 0.5	Variable
	Mg II	sdss	2010		−9.2 ± 0.6	
	Mg II	sdss	2011		−9.1 ± 0.4	
	Mg II	sdss	2008		−12.5 ± 1.1	
	Mg II	sdss	2009		−12.3 ± 1.0	

Table 5 – *continued*

Name	Ion	Epoch ID 1	Epoch ID 2	λ range (Å)	Ratio	Comments
	Mg II	sdss	2010	6279.1–6464.1	−11.9 ± 2.0	
SDSS J0952+0257	Mg II	sdss	2011		−11.0 ± 1.2	Variable
	Al III	sdss	2008		−5.4 ± 0.9	
	Al III	sdss	2009	4211.9–4293.1	−4.8 ± 0.8	
	Al III	sdss	2010		−8.5 ± 2.0	
	Al III	sdss	2011		−4.4 ± 1.1	
	Al III	sdss	2008		2.2 ± 1.1	
SDSS J1010+4518	Al III	sdss	2009	4939.1–5061.4	0.9 ± 1.1	
	Al III	sdss	2010		3.3 ± 1.1	
	Mg II	sdss	2010		−3.7 ± 0.9	
SDSS J1128+4823	Mg II	sdss	2011	4228.9–4330.4	−1.4 ± 0.9	
	Mg II	2010	2011		2.7 ± 1.1	
	Al III	sdss	2008		1.7 ± 1.7	
SDSS J1143+5203	Al III	2008	2009	7770.1–7848.9	−0.5 ± 1.4	
	Mg II	sdss	2010		−2.3 ± 0.3	
SDSS J1208+0230	Mg II	sdss	2011	5743.2–5813.1	−1.9 ± 0.3	Variable
	Mg II	2010	2011		0.2 ± 0.3	
	Mg II	2000	2001		−1.1 ± 0.2	
	Mg II	2000	2008		−3.6 ± 0.7	
SDSS J1333+0012	Mg II	2000	2009(7)†	5035.7–5090.9	−3.8 ± 0.3	Variable
R component	Mg II	2000	2009(1)†		−5.6 ± 0.5	
	Mg II	2000	2010		−6.3 ± 0.3	
	Mg II	2000	2011		−6.9 ± 0.5	
	Mg II	2000	2001		4.3 ± 0.4	
	Mg II	2000	2008		18.9 ± 1.3	
SDSS J1333+0012	Mg II	2000	2009(7)†	4790.7–5000.9	31.5 ± 0.5	Variable
B component	Mg II	2000	2009(1)†		28.2 ± 1.0	
	Mg II	2000	2010		19.3 ± 0.4	
	Mg II	2000	2011		8.0 ± 0.9	
	Al III	sdss1	2008		−3.4 ± 1.3	
SDSS J1334−0123	Al III	sdss1	2009	5142.5–5302.9	−1.2 ± 0.9	
	Al III	sdss1	sdss2		0.3 ± 1.4	
	Mg II	sdss1	2010		1.9 ± 0.9	
	Mg II	sdss1	2011	6979.6–7064.4	2.6 ± 0.6	
	Mg II	sdss1	sdss2		1.4 ± 0.4	
SDSS J1448+0424	Al III	sdss1	2010		1.5 ± 1.2	
	Al III	sdss1	2011	4624.1–4698.8	3.2 ± 0.6	
	Al III	sdss1	sdss2		2.0 ± 0.4	
	Mg II	sdss	2008		−1.3 ± 0.5	
SDSS J1614+3752	Mg II	sdss	2010	4250.4–4301.4	−0.7 ± 0.4	
	Mg II	sdss	2011		−0.2 ± 0.4	
	Mg II	sdss	vlt		−3.0 ± 0.6	
	Mg II	sdss	2008		−8.3 ± 0.6	Variable
SDSS J2215−0045	Mg II	sdss	mage	6512.2–6735.2	−7.6 ± 1.8	
	Mg II	sdss	2011		−7.5 ± 1.0	
	Al III	sdss	vlt		−21.2 ± 0.6	
	Al III	vlt	2008		−37.0 ± 0.8	
	Al III	2008	2010	4345.0–4419.6	−37.5 ± 1.3	
	Al III	2010	mage		−36.2 ± 0.9	
	Al III	Mage	2011		−36.6 ± 1.2	
	Mg II	sdss1	sdss2	7448.6–7716.4	0.8 ± 1.2	
SDSS J2347−1037	Al III	sdss1	sdss2		−4.0 ± 0.9	
	Al III	2008	2008	4932.0–5110.4	−1.0 ± 1.3	
	Al III	2009	2009		2.8 ± 2.7	

†7 and 1 in the parentheses refer to IFOSC 7 and IFORS 1 data, respectively.
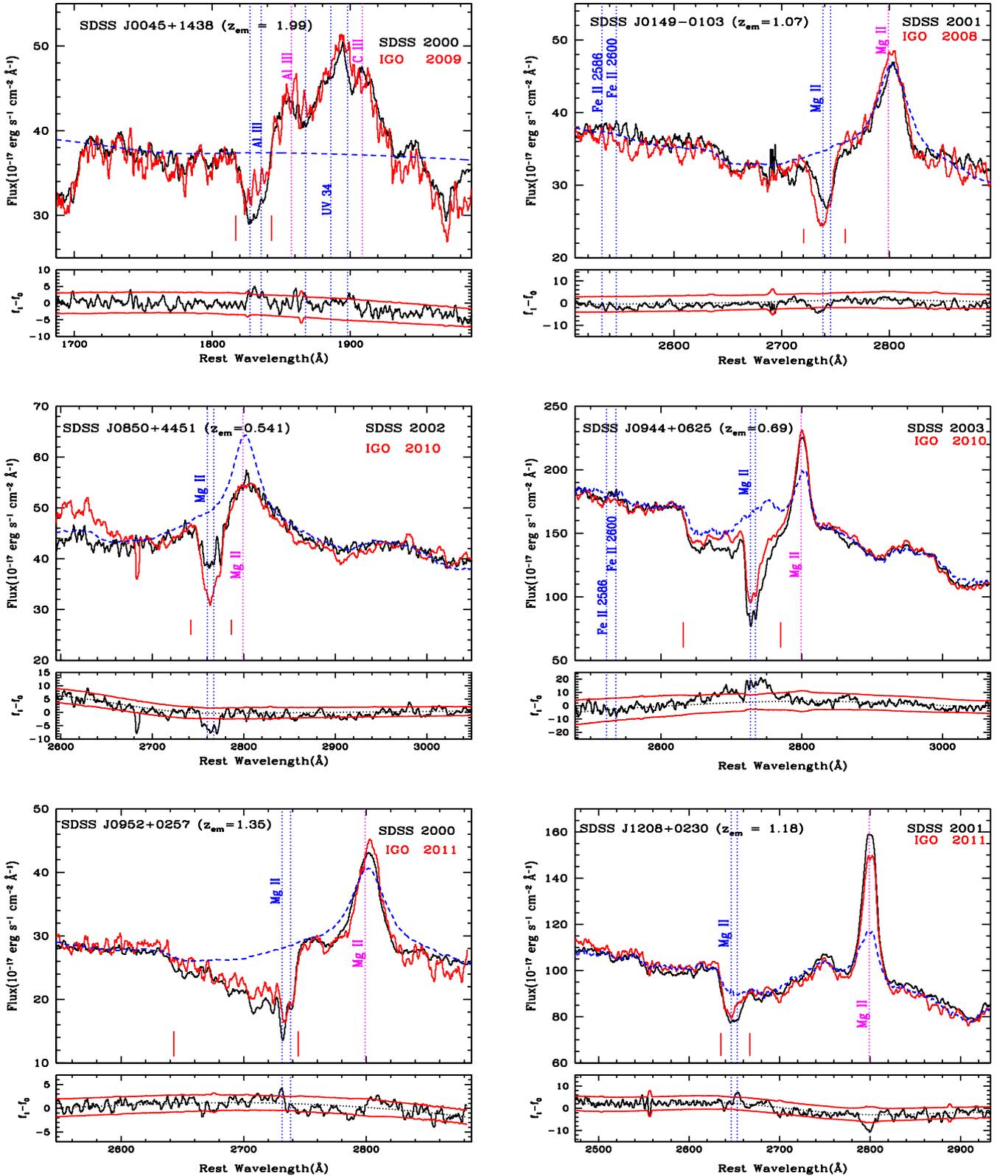
Figure 4. Comparison of IGO and SDSS spectra for the varying BAL QSOs discussed in Section 4. The flux scale applies to the reference SDSS spectrum and all other spectra are scaled in flux to match the reference. Blue (long dashed) spectra represent the continuum used for normalization. The difference spectrum for the corresponding MJDs is plotted in the lower panel of each plot. 1σ error is plotted above and below the mean. Magenta vertical lines (long dashed) mark the locations of emission lines and blue vertical lines (dotted) mark the locations of absorption lines (maximum optical depth). Two vertical red lines below the spectra mark the locations of V_{max} and V_{min}.
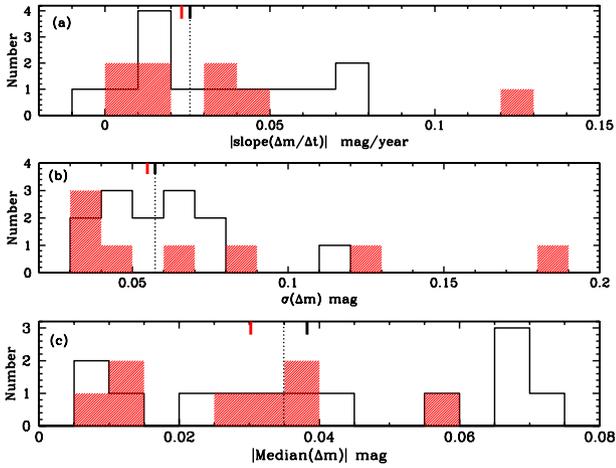
Figure 5. The three panels show the histogram distribution of (a) absolute values of slopes $(\Delta m/\Delta t)$ (b) standard deviation of the magnitude differences and (c) absolute median of the magnitude differences for sources with variable and non-variable BALs. The line histogram corresponds to sources with non-variable BALs and the red shaded histogram corresponds to sources with variable BALs. The median values for the two distributions are marked at the top in black and red, respectively. It is clear that objects with variable and non-variable BALs appear to be drawn from the same distribution in terms of continuum variability.

Figure 6. Variation of ΔW with Δt for Mg II absorption. Red triangles mark the two sources with dramatically varying BALs. The blue (solid) and magenta (dot dashed) curve represents the variation of rms differences computed in bins containing six time-scale values with and without the inclusion of the sources showing dramatic BAL variability, respectively. Orange (dashed) curve represents the variation of rms differences with time-scales for Al III.

our equivalent width and ratio measurements. Four sources, SDSS J0149−0103, SDSS J0944+0625, SDSS J1208+0230 and SDSS J2215−0045, have shown significant variability in Mg II BAL equivalent widths. The Al III absorption line is covered only in SDSS J2215−0045, which has varied. We note that iron emitting sources are among the top ones in the whole sample showing maximum variations in the absorption lines. The percentage of sources with variable BALs in this iron emitter sub-sample is about 50 per cent (4/8). Out of the 14 remaining sources which do not show strong iron emission, four (i.e. 29 per cent) show variations.

5.2 Correlation with photometric parameters

To understand the correlation of the BAL variations with continuum parameters, we split the whole sample into two sub-samples of objects with and without BAL variations. Fig. 5 shows the histogram distribution of various photometric parameters for the two groups. The line histogram corresponds to the sample of non-varying BALs and the shaded histogram corresponds to the sample of varying BALs. Panel (a) shows the histogram distribution for the absolute slope values. Panels (b) and (c) show distributions for the standard deviation and the absolute median values of the magnitude differences. The median values for the two distributions are marked at the top of each panels and the median value for the whole sample is marked by dotted vertical lines. It is clear from Fig. 5 that the distribution of the photometric parameters for the samples with and without absorption line variations of BALs is similar. Two-sided Kolmogorov–Smirnov (KS) test for these distributions results in D and probability values of (0.2, 95 per cent), (0.3, 69 per cent) and (0.4, 36 per cent). This implies both the sub-samples are drawn from the same parent population. We also find the structure function computed for the above two sub-samples to be similar within the measurement uncertainties. Similarity of photometric parameter distribution for the two samples implies that the BAL QSOs showing absorption line variations are not associated with a particular range in the values of any of these photometric parameters.

5.3 Variation of equivalent widths with time-scales

Gibson et al. (2008), Capellupo et al. (2012) and Filiz Ak et al. (2013) studied the variation of C IV equivalent widths with time and reported that longer the time-scale, larger is the variation in the equivalent widths. The C IV variability probability approaches unity when $\Delta t \geq 10$ yr. From the discussions presented in Section 4, we notice that, even among sources with varying absorption lines, only 50 per cent of them show variation over shorter time-scales (i.e. <1 yr in the QSO rest frame). Fig. 6 shows the plot of the variation of absolute Mg II ΔW with Δt in the QSO rest frame. Though only eight sources show >3σ variations, all the variations between epochs are considered here. As the variation in two sources, namely SDSS J1333+0012 and SDSS J2215−0045, is exceptionally high, they were observed more frequently and hence they contribute more than others in the plot. This will also lead to a clustering of measurements at shorter time-scales. We do not have any preferential sampling of measurements for the rest of the objects. The red triangles mark the locations of these two sources in the plot. The blue (solid) and magenta (dot–dashed) curve represents the variation of rms of equivalent width differences computed in six time-scale bins with and without the inclusion of two sources with highly varying BALs, respectively. The inclusion of these two sources does not change the overall trend. It is clear from the figure that Mg II LoBAL QSOs also tend to show large amplitude variations over long time-scales. The increased incidence of variability at larger time-scales indicates that the physical process causing the BAL variations is a slow one which dominates over multi-year time-scales. Orange (dashed) curve in the top panel shows a similar plot of variation of ΔW for Al III. There is no clear indication of any trend in the variation over different time-scales.

5.4 Variation of equivalent width with mean equivalent width $\langle W \rangle$

Here, we explore the dependence of Mg II BAL variability on the overall strength of the BAL absorption. Previous studies on the
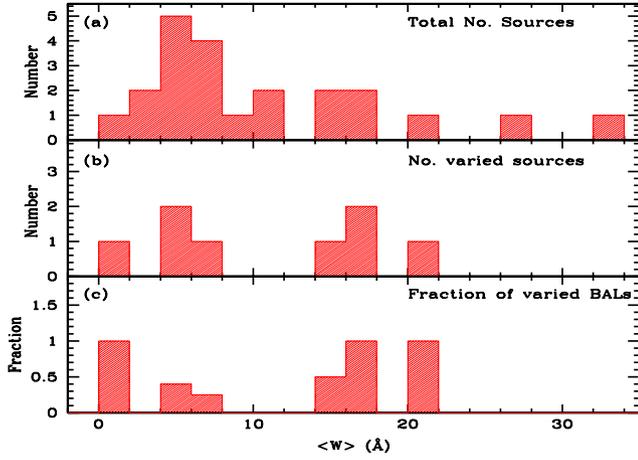
Figure 7. Panels (a) and (b) show the number of QSOs with Mg II BAL absorption and the number with Mg II BAL variability at each absorption strength. Panel (c) shows the fraction of Mg II BALs that have varied at each absorption strength. Clearly there is no evidence for high fractional variation among BALs with low Mg II equivalent widths.

In Fig. 7, the top two panels (a) and (b) show the number of QSOs with Mg II BAL absorption and the number with Mg II BAL variability at each absorption strength. Panel (c) shows the fraction of Mg II BALs that have varied at each Mg II equivalent width. Clearly, there is no evidence for high fractional variation among BALs with low Mg II equivalent widths. In Fig. 8, panel (a) shows the absolute variation of the fractional change in the equivalent widths with the mean equivalent width for Mg II BALs. The blue circles represent the sources that show BAL variability. Here, we have considered all the possible pairs of equivalent width measurements for each QSOs. In Fig. 10, panel (a) shows the absolute fractional variation of the Al III equivalent widths with the average BAL equivalent widths. From these plots, it is clear that both Mg II and Al III show more scatter at low equivalent widths as has been reported for C IV BALs. But, in the case of Mg II systems, one source, SDSS J1333+0012, dominates the results. The correlation is more prominent in Al III as compared to Mg II. The wavelength range where Mg II absorption is observed is significantly affected by iron emission features whereas it is not the case for Al III. Strong iron features which contaminate the Mg II regions could be the reason for the weakness of this correlation in Mg II BALs.

correlation between C IV BAL equivalent width variation and absorption strength have reported that weaker portions of BAL troughs are more likely to vary than stronger ones (see Barlow 1994; Lundgren et al. 2007; Gibson et al. 2008; Capellupo et al. 2011).

5.5 Dependence of variation in equivalent width with V_{max}

C IV BAL absorption, on an average, is found to be shallower at highest velocities. If these systems are less saturated, high-velocity
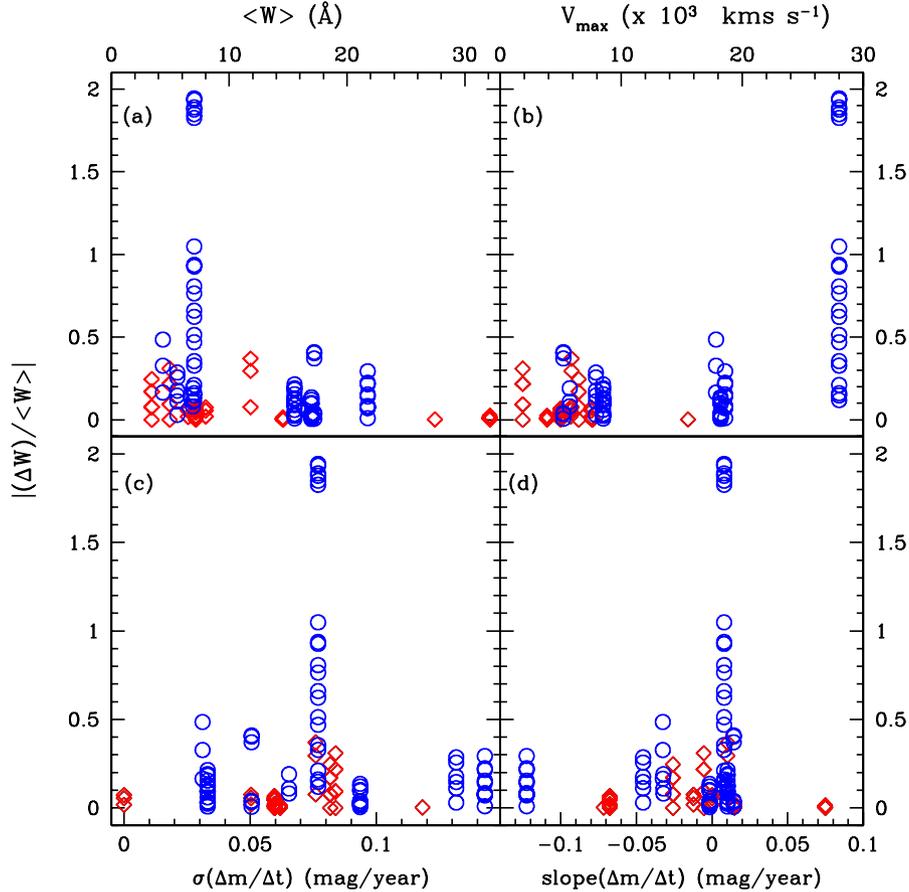
Figure 8. Fractional variation of Mg II equivalent widths are plotted against $\langle W \rangle$, V_{max}, $\sigma(\Delta m/\Delta t)$ and slope of the $\Delta m - \Delta t$ curve in panels a, b, c and d, respectively. The blue circular and red diamond points mark the values for the sources with varying BALs and non-varying BALs. It is clear that Mg II equivalent widths show more scatter at low equivalent widths and high velocities whereas no correlation is seen with continuum parameters.
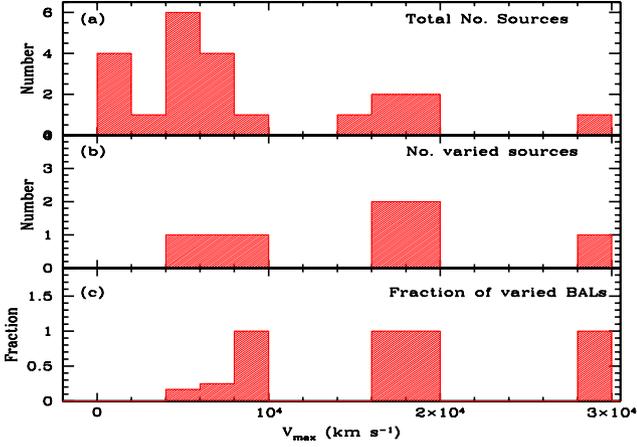
Figure 9. The top two panels show the number of QSOs with Mg II BAL absorption and the number with Mg II BAL variability at each V_{max}. The lower panel shows the fraction of Mg II BALs that have varied at each V_{max}. The plot clearly points to the correlation between the variations in BAL absorption and the outflow velocities.

BALs can be more responsive to ionization changes. Lundgren et al. (2007) do not find any linear relationship between the equivalent width variability and the BAL velocity. But, they note that the most highly variable BALs in their sample are found at high velocities. Gibson et al. (2008) also do not find any indications for the variation

of ΔW across the velocity ranges. Capellupo et al. (2011) find that components at higher velocity are more likely to vary than those at lower velocities. But, they do not find any statistically significant trend between fractional change in absorption strength and the outflow velocity.

In Fig. 9, the two panels (a) and (b) show the number of quasars with Mg II BAL absorption and the number with Mg II BAL variability at each velocity. Panel (c) shows the distribution of variable sources with outflow velocities. Though the smaller velocity bins have more number of sources, the varying fraction is small. This clearly points to the correlation between the variations in BAL absorption and the outflow velocities. The observed correlation is again reiterated by the panel (b) of Fig. 8 where the absolute fractional variation of the Mg II equivalent widths is plotted against the velocities. Panel (b) of Fig. 10 shows the absolute fractional variation of the Al III equivalent widths with the V_{max}. Our Al III BAL sub-sample does not contain many sources at high velocities. Only one source, SDSS J2215−0045, has varied significantly at high velocity. Here, there is no apparent correlation evident between the two parameters within the available Al III velocity ranges. Overall, this study also points to higher incidence of sources with variable BALs at high outflow velocities, which has been observed in the case of HiBALs. If the broad absorption troughs originate in a radiatively driven wind, a relation between luminosity and V_{max} is expected. Studies of Laor & Brandt (2002), Ganguly et al. (2007) and Stalin et al. (2011) on C IV absorption systems confirm a luminosity-dependent envelope to the maximum velocity of
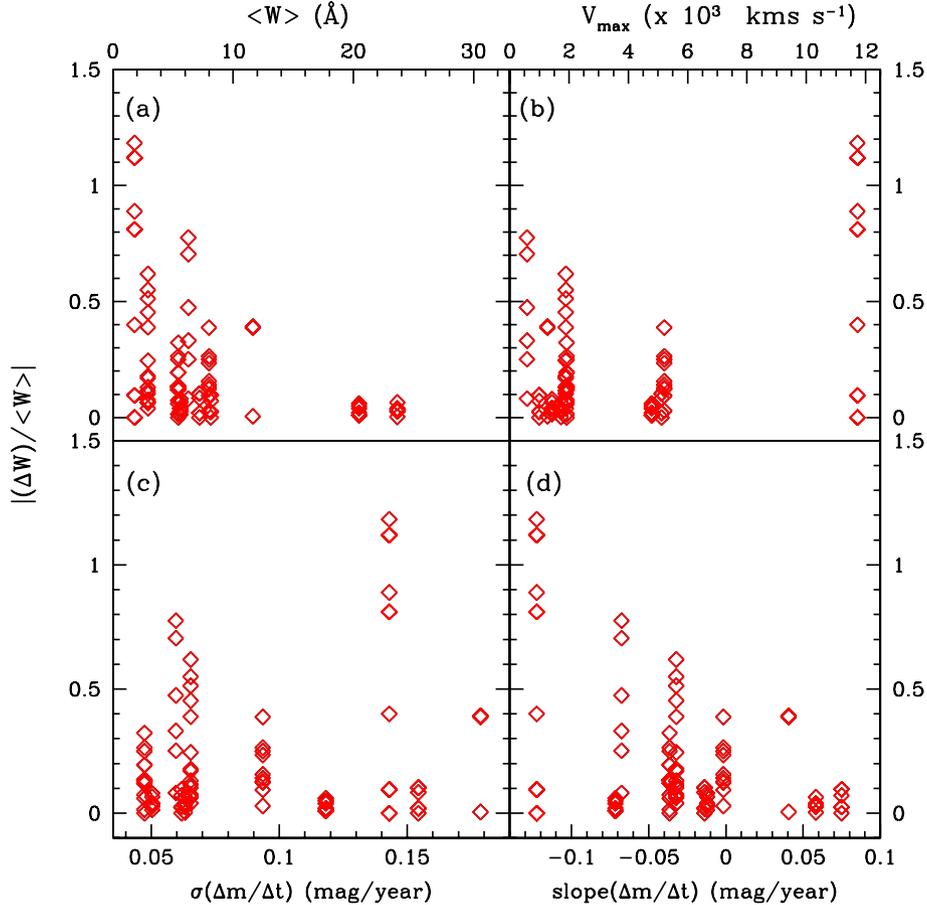

Figure 10. Same as in Fig. 8, but for Al III. Here again, Al III equivalent widths show more scatter at low equivalent widths pointing to a correlation between them. But the correlations with V_{max} and continuum parameters are not seen.
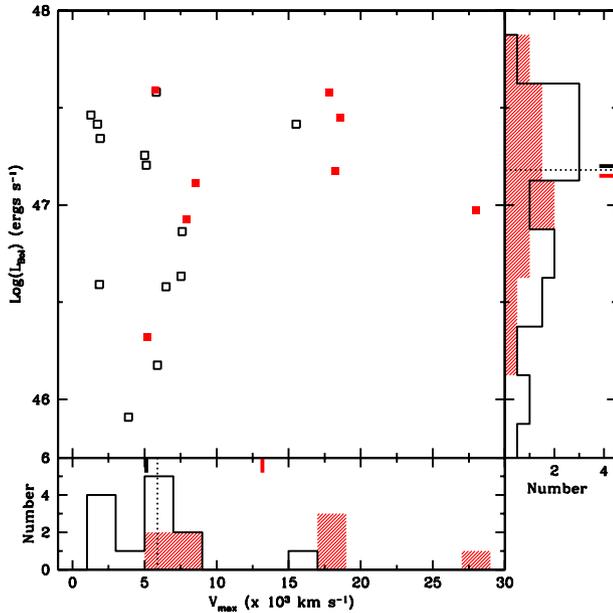
Figure 11. Bolometric luminosity is plotted against the maximum outflow velocity. Open and filled squares mark the sources with non-varying and varying BALs. Velocity histogram distribution for the samples with varying (shaded histogram) and non-varying (line histogram) BALs is shown in the lower panel and luminosity histogram distribution for the same samples are shown on right panel. Note that high fraction of varying BAL objects occupy the high velocity high luminosity quadrant.

absorption. In Fig. 11, bolometric luminosity for each source is plotted against its outflow velocity. Open and filled squares mark the sources with non-varying and varying BALs, respectively. Similar to what is seen in C IV BALs, LoBAL QSOs in this study also show a lower envelope. The left and bottom side panels show the histogram distributions of velocities and luminosities for the samples with varying (red) and non-varying (black) BALs. The dotted line in these side panels marks the median of the whole sample. Black and red/grey ticks at the top of the histogram panels mark the median value of the non-varying and varying samples, respectively. From the velocity distributions in the lower panel, it is clear that the varying and non-varying samples are different. The median velocity of the varying sample is at a higher velocity as compared to the non-varying sample. However, we do not find difference between the luminosity distributions of the varying and non-varying samples (see left panel of Fig. 11). This could mean that the variations in BALs are not affected by the strength of QSO luminosity. However, it is interesting to note that a high fraction of objects in the high velocity high luminosity quadrant of Fig. 11 show variability.

5.6 Dependence of BAL variation on the continuum

One natural possibility that has been invoked to explain absorption line variability in BALs is the variations in the continuum. Changes in the continuum fluxes can be correlated with the variations in BALs mainly in three ways. Changes in the far-UV continuum flux can directly change the ionizing conditions of the outflowing gas and it will reflect as variations in the BAL optical depths. In the simplest form of photoionization models, one expects an overall absorption profile change. Therefore, BAL variations across the complete absorption profiles are usually attributed to ionization changes. Another possibility is the luminosity induced dynamical changes in the absorbing gas. If radiation pressure is driving the

outflows, it is natural to think that the changes in the luminosity can shift the absorptions to higher/lower velocities (Srianand 2000). Vivek et al. (2012a) discussed about another possibility where the structural changes in the accretion disc result in changes in the continuum and BAL absorptions. This could mean the ejection being triggered by some events in the accretion disc that caused reduction in the accretion efficiency. Appearance/disappearance of new BAL components can be thought of resulting from this structural changes in the accretion disc.

The inverse correlation between the BAL variability and the ⟨*W*⟩ suggests a mechanism driven by changes in the continuum ionization. Since larger equivalent width BAL profiles are more likely to be saturated, changes in the continuum may not affect the strong BAL absorption significantly. Previous studies on continuum variability in BAL QSOs have found no conclusive evidence for the dependence of the absorption line variations on continuum flux changes. Barlow (1994) found some marginal evidence of correspondence between these parameters. But, they also reported high frequency of exceptions to this correlation. Lundgren et al. (2007) found that there is no correlation between BAL variations and the 1549 Å flux variability. Gibson et al. (2010) took the C IV emission line flux as a proxy to the continuum and found significant correlations between continuum flux and absorption line equivalent widths. However, none of these studies could use long-term photometric light curves.

In our study, the continuum and absorption line observations almost span the same time period. From the CRTS light curves, we obtained the *V* magnitudes of each sources at the same epoch of spectroscopic measurements. These magnitudes are used to compute the differences. In Figs 8 and 10, the absolute values of Mg II and Al III fractional equivalent widths are plotted against the different parameters of continuum variability in the lower two panels. In panel (c) of both the figures, we have plotted fractional variation in equivalent widths against the standard deviation of time averaged differences in magnitudes, i.e. $\Delta m / \Delta t$, between various epochs. A larger value for the standard deviation means a higher rate for continuum variation. In panel (d) of the two figures, we have plotted the equivalent width fractional variation against the slope of the $\Delta m - \Delta t$ curve. We do not find any trend in the variation of the Mg II and Al III BAL equivalent widths with the continuum parameters.

Although we do not detect any strong correlation between the continuum and BAL variations in the sample, some of the sources are promising candidates for the scenarios discussed in the beginning of this section. As discussed earlier, in SDSS J0149−0103, SDSS J1208+0230 SDSS J1333+0012 and SDSS J2215−0045, the observed variations are consistent with dynamical changes in the absorbing clouds. SDSS J1333+0012 is a good example for the scenario of structural changes in the accretion disc. The observed variations in SDSS J0850+4452 and SDSS J0952+0257 are consistent with the scenario of changing ionization. In reality, it can be a mixture of all these effects contributing to the variations in the absorption profiles.

6 RESULTS AND CONCLUSIONS

We have presented a detailed analysis of a sample of 22 LoBAL QSOs that are monitored both spectroscopically and photometrically over a period of a few days to a few years in the QSO rest frame. Most of the results are based on equivalent widths, but we show that they are consistent with results from a spectral ratio analysis that avoids problems related to the continuum fitting. The main results from the study are summarized below.

(i) Out of 22 BALs monitored, eight are showing absorption line variability. We define a variable BAL as the one with variations in rest equivalent width $>3\sigma$ level and ratio $>5\sigma$. Gibson et al. (2008) and Capellupo et al. (2011), in their studies on C IV BALs, reported the fraction of varying BALs to be 92 per cent and 67 per cent, respectively. Very recently, Filiz Ak et al. (2013) have found 50–60 per cent of C IV BALs showing variability over a time-scale of 1–3.7 years using an extended sample from SDSS. As compared to the C IV BALs, the fraction of varying BALs in our overall sample is small (i.e. 36 per cent). Capellupo et al. (2011) used a slightly higher threshold (4σ) to define the variability and their sample span the redshift range $1.2 < z < 2.9$. In this redshift range, the variability detection is even less (i.e. 25 per cent) for our LoBAL QSO sample.

(ii) We find a greater incidence of variability at long time-scales (>1 yr) than short time-scales (<1 yr). Capellupo et al. (2011) find that 39 per cent of C IV BALs varied in the short-term data, whereas 65 per cent varied in the long-term data. In this study of Mg II BALs, we find the respective variable fraction to be 18 per cent and 36 per cent for short-term and long-term data. This could mean that the physical process causing the BAL variations dominates over multi-year time-scales.

(iii) In two sources, SDSS J1333+0012 and SDSS J2215−0045, there is appearance/disappearance of BAL components. The observed frequency of 9 per cent for BAL appearance/disappearance is different from the value, 3 per cent found for C IV BALs (Filiz Ak et al. 2012). Confirming this possible difference is important for understanding the different BAL QSO classes in the frame work of 'orientation' or 'evolutionary' scenario.

(iv) As has been reported for C IV BALs, we also find a trend for larger fractional change in absorption equivalent widths to occur in shallower and higher velocity features. We do not find any correlation between BAL variations and the QSO luminosity. However, it is interesting to note that there is a higher fraction of objects in the high-velocity high-luminosity range.

(v) The observed fraction of sources with varying BALs in FeLoBAL QSOs (i.e. 20 per cent) is small compared to LoBAL QSOs (44 per cent) and HiBALs (67 per cent). Our observation suggests that FeLoBAL QSOs could be a different population compared to LoBAL QSOs not showing Fe II absorption. Such a difference is expected based on dust emission and distance estimates of clouds from photoionization models. However, as the predictions for the variability time-scales are not available, we are not in a position to distinguish between the two proposed scenarios of FeLoBAL QSOs.

(vi) We find a larger fraction of sources with varying BALs in a sub-sample of Fe emitting sources. Zhang et al. (2010) have found that the LoBAL QSO fraction is higher when the strength of Fe II emission is high using SDSS-DR5 data. Dong et al. (2011) have found a strong correlation between Fe II emission strength and Eddington ratio. Confirming the higher variability detection in BAL QSOs with Fe II dominated continuum in a larger sample will establish the connection between Eddington ratio (i.e. accretion efficiency) and line variability.

(vii) We do not find any trend in the variation of the Mg II and Al III BAL equivalent widths with the continuum parameters. This is consistent with what is seen in previous studies on C IV BAL systems. Wide range in equivalent width differences, ΔW, seen for a given magnitude difference, Δm and vice versa imply that absorption line variations are not dominantly driven by photo-ionization changes induced by continuum variations. Emergence and profile variations of BALs in some sources imply that dynamical changes like movement of clouds across the line of sight may be important.

REFERENCES

Allen J. T., Hewett P. C., Maddox N., Richards G. T., Belokurov V., 2011, MNRAS, 410, 860

Aoki K., Oyabu S., Dunn J. P., Arav N., Edmonds D., Korista K. T., Matsuhara H., Toba Y., 2011, PASJ, 63, 457

Arav N., Li Z.-Y., Begelman M. C., 1994, ApJ, 432, 62

Arav N., Korista K. T., Barlow T. A., Begelman, 1995, Nature, 376, 576

Barlow T. A., 1994, PASP, 106, 548

Barlow T. A., Junkkarinen V. T., Burbidge E. M., 1989, ApJ, 347, 674

Barlow T. A., Junkkarinen V. T., Burbidge E. M., Weymann R. J., Morris S. L., Korista K. T., 1992, ApJ, 397, 81

Bautista M. A., Dunn J. P., Arav N., Korista K. T., Moe M., Benn C., 2010, ApJ, 713, 25

Becker R. H., Gregg M. D., Hook I. M., McMahon R. G., White R. L., Helfand D. J., 1997, ApJ, 479, L93

Becker R. H., White R. L., Gregg M. D., Brotherton M. S., Laurent-Muehleisen S. A., Arav N., 2000, ApJ, 538, 72

Borguet B., Hutsemékers D., 2010, A&A, 515, A22

Borguet B. C. J., Edmonds D., Arav N., Dunn J., Kriss G. A., 2012, ApJ, 751, 107

Borguet B. C. J., Arav N., Edmonds D., Chamberlain C., Benn C., 2013, ApJ, 762, 49

Capellupo D. M., Hamann F., Shields J. C., Rodríguez Hidalgo P., Barlow T. A., 2011, MNRAS, 413, 908

Capellupo D. M., Hamann F., Shields J. C., Rodríguez Hidalgo P., Barlow T. A., 2012, MNRAS, 422, 3249

de Kool M., Begelman M. C., 1995, ApJ, 455, 448

de Vries W. H., Becker R. H., White R. L., Loomis C., 2005, AJ, 129, 615

Dong X.-B., Wang J.-G., Ho L. C., Wang T.-G., Fan X., Wang H., Zhou H., Yuan W., 2011, ApJ, 736, 86

Drake A. J. et al., 2009, ApJ, 696, 870

Dunn J. P. et al., 2010, ApJ, 709, 611

Elvis M., 2000, ApJ, 545, 63

Fan L. L., Wang H. Y., Wang T., Wang J., Dong X., Zhang K., Cheng F., 2009, ApJ, 690, 1006

Farrah D., Lacy M., Priddey R., Borys C., Afonso J., 2007, ApJ, 662, L59

Faucher-Giguère C.-A., Quataert E., Murray N., 2012, MNRAS, 420, 1347

Ferrarese L., Merritt D., 2000, ApJ, 539, L9

Filiz Ak N. et al., 2012, ApJ, 757, 114

Filiz Ak N. et al., 2013, ApJ, 777, 168

Foltz C. B., Weymann R. J., Morris S. L., Turnshek D. A., 1987, ApJ, 317, 450

Gallagher S. C., Brandt W. N., Chartas G., Priddey R., Garmire G. P., Sambruna R. M., 2006, ApJ, 644, 709

Ganguly R., Brotherton M. S., Cales S., Scoggins B., Shang Z., Vestergaard M., 2007, ApJ, 665, 990

Ghosh K. K., Punsly B., 2007, ApJ, 661, L139

Gibson R. R., Brandt W. N., Schneider D. P., Gallagher S. C., 2008, ApJ, 675, 985

Gibson R. R., Brandt W. N., Gallagher S. C., Schneider D. P., 2009, ApJ, 696, 924

Gibson R. R., Brandt W. N., Gallagher S. C., Hewett P. C., Schneider D. P., 2010, ApJ, 713, 220

Green P. J. et al., 1995, ApJ, 450, 51

Hall P. B., Anosov K., White R. L., Brandt W. N., Gregg M. D., Gibson R. R., Becker R. H., Schneider D. P., 2011, MNRAS, 411, 2653

Hamann F., Kaplan K. F., Rodríguez Hidalgo P., Prochaska J. X., Herbert-Fort S., 2008, MNRAS, 391, L39

Hewett P. C., Foltz C. B., 2003, AJ, 125, 1784

Korista K. T., Bautista M. A., Arav N., Moe M., Costantini E., Benn C., 2008, ApJ, 688, 108

Lamy H., Hutsemékers D., 2004, A&A, 427, 107

Laor A., Brandt W. N., 2002, ApJ, 569, 641

Lazarova M. S., Canalizo G., Lacy M., Sajina A., 2012, ApJ, 755, 29

Lundgren B. F., Wilhite B. C., Brunner R. J., Hall P. B., Schneider D. P., York D. G., Vanden Berk D. E., Brinkmann J., 2007, ApJ, 656, 73

MacLeod C. L. et al., 2012, ApJ, 753, 106

Marconi A., Risaliti G., Gilli R., Hunt L. K., Maiolino R., Salvati M., 2004, MNRAS, 351, 169

Moe M., Arav N., Bautista M. A., Korista K. T., 2009, ApJ, 706, 525

Murray N., Chiang J., Grossman S. A., Voit G. M., 1995, ApJ, 451, 498

Muzahid S., Srianand R., Savage B. D., Narayanan A., Mohan V., Dewangan G. C., 2012, MNRAS, 424, L59

Muzahid S., Srianand R., Arav N., Savage B. D., Narayanan A., 2013, MNRAS, 431, 2885

Pâris I. et al., 2012, A&A, 548, A66

Proga D., Kallman T. R., 2004, ApJ, 616, 688

Proga D., Stone J. M., Kallman T. R., 2000, ApJ, 543, 686

Reichard T. A. et al., 2003, AJ, 125, 1711

Richards G. T., Vanden Berk D. E., Reichard T. A., Hall P. B., Schneider D. P., SubbaRao M., Thakar A. R., York D. G., 2002, AJ, 124, 1

Rupke D. S., Veilleux S., Sanders D. B., 2002, ApJ, 570, 588

Silk J., Rees M. J., 1998, A&A, 331, L1

Smith L. J., Penston M. V., 1988, MNRAS, 235, 551

Srianand R., 2000, ApJ, 528, 617

Srianand R., Petitjean P., 2001, A&A, 373, 816

Srianand R., Petitjean P., Ledoux C., Hazard C., 2002, MNRAS, 336, 753

Srianand R., Gupta N., Petitjean P., Noterdaeme P., Saikia D. J., 2008, MNRAS, 391, L69

Stalin C. S., Srianand R., Petitjean P., 2011, MNRAS, 413, 1013

Trump J. R. et al., 2006, ApJS, 165, 1

Turnshek D. A., Grillmair C. J., Foltz C. B., Weymann R. J., 1988, ApJ, 325, 651

Vilkoviskij E. Y., Irwin M. J., 2001, MNRAS, 321, 4

Vivek M., Srianand R., Noterdaeme P., Mohan V., Kuriakosde V. C., 2009, MNRAS, 400, L6

Vivek M., Srianand R., Mahabal A., Kuriakose V. C., 2012a, MNRAS, 421, L107

Vivek M., Srianand R., Petitjean P., Noterdaeme P., Mohan V., Mahabal A., Kuriakose V. C., 2012b, MNRAS, 423, 2879

Wampler E. J., Chugai N. N., Petitjean P., 1995, ApJ, 443, 586

Welsh B. Y., Wheatley J. M., Neil J. D., 2011, A&A, 527, A15

Weymann R. J., Morris S. L., Foltz C. B., Hewett P. C., 1991, ApJ, 373, 23

Zhang S., Wang T.-G., Wang H., Zhou H., Dong X.-B., Wang J.-G., 2010, ApJ, 714, 367

APPENDIX A: NOTES ON INDIVIDUAL VARIABLE BAL SOURCES

In this section, we discuss individual QSOs that have shown significant variability of the BALs. The plots depicting variabilities in these sources are given in Fig. 4. The absorption line variabilities can be compared to the variations in the continuum. As the CRTS survey does not cover SDSS epochs for sources in our sample, comparison between the absorption line and continuum variations

is better done when absorption line variations are seen between IGO epochs.

A1 SDSS J0045+1438

As the Mg II absorption in this case falls in the wavelength range just outside the IFOSC/GR8 coverage, we only study the variability of Al III and C IV absorption lines using our IGO data. The optical-UV SED fitting using both the SDSS composite and the Fe template did not give good fits to the continuum. Hence, a simple polynomial fit is used to approximate the continuum. SDSS has three epochs of data. The Mg II line is only covered in the SDSS spectrum and has a maximum ejection velocity of $\sim$5800 km s^{-1}. This source does not show any variability in any of the absorption lines between different SDSS epochs. But, there are variations seen in Al III line between SDSS and IGO epochs (see Figs 4 and C1). The absorption line has decreased in optical depth in the IGO spectrum as compared to those observed in SDSS. Even within the IGO epochs, the Al III absorption continued to weaken between the years 2007 and 2009. Both the equivalent width measurements and the integrated ratio values point to similar trends in variations. We detect 5σ variation in Al III equivalent widths between SDSS and IGO spectrum observed in 2009 (see Table 4) epoch. A similar trend in variation is also seen in the C IV lines. The ratio values point to changes at about 4σ level (see Table 5) between the SDSS and IGO epochs, but not between different IGO epochs. The light curve of this source shows a small decrease in the magnitudes over the CRTS monitoring period. But, no significant variability over the period of IGO spectroscopic monitoring (see Fig. B1). There is also no difference seen in the fibre magnitudes for the SDSS epochs. The scatter in the Δm values is 0.04 around a median value of -0.04. The $\Delta m - \Delta t$ graph has no significant slope. All the continuum parameters point to no appreciable variation in the continuum flux for this source. Therefore, it is most unlikely that the noted variation in Al III and C IV absorption lines is caused by a change in the ionization state of the gas.

A2 SDSS J0149−0103

The emission redshift of the source is 1.0740. The Mg II BAL without having associated Fe II absorption is at a redshift of 1.0320 and a maximum ejection velocity of 7900 km s^{-1}. There is a narrow intervening Mg II absorption at a redshift of 0.428. We fitted the continuum using the SDSS quasar composite as the template. The Mg II absorption has deepened in 2008 and 2009 IGO spectra as compared to that seen in the SDSS spectrum (see Figs 4 and C2). Between the IGO epochs 2008 and 2009, the absorption has not changed. SDSS BOSS survey has re-observed this source in 2010. The absorption decreased in strength in 2010 and continued to weaken in the IGO spectrum observed in 2012. This trend is clearly seen both in the equivalent width measurements (see Table 4) and in the integrated ratio measurements (see Table 5). The maximum variation is seen between the epochs 2009 and 2012. We detect more than 3σ variation in equivalent widths and 7σ variation in the integrated ratio values. This is a clear case of confirmed variations between the epochs, even within short time-scales probed by the IGO observations. As can be seen from Fig. 4, it appears that, for the strongest absorption component, the peak optical depth is blueshifted by about $\sim$440 km s^{-1} in IGO observations as compared to that seen in the original SDSS data. However, no such shifts is noted between spectra obtained in different IGO epochs.

The CRTS light curve clearly shows significant variations in the continuum flux. There is a coherent trend of initial decrease in the continuum flux followed by the brightening of the source (see Fig. B1) in the CRTS light curve. We notice that between SDSS and the first IGO observation, the QSO has become faint, in line with the trend seen in CRTS. Our IGO spectroscopic observations are mostly during the phase when the QSO has brightened. The standard deviation and the median of the magnitude differences are 0.13 and -0.01. Large scatter in the magnitude differences implies large variations in the magnitudes at all time-scales. The $\Delta m - \Delta t$ slope is -0.046 ± 0.007 mag yr^{-1}. This source clearly suggests a possible correlation between the absorption line and continuum variations. The Mg II absorption line optical depth gained in strength when the source weakened in continuum and vice versa. We have reported a similar variation for the source SDSS J1333+0012 (Vivek et al. 2012a) where the source displayed opposite trends in variations of the QSO flux and the Mg II BAL column densities. Like in that case, correlated variability between optical depth and continuum light suggests a possible connection between them. However, wavelength shift seen for the peak optical depth noted between SDSS and IGO data suggests that the changes may not purely be triggered by ionization changes.

A3 SDSS J0850+4451

The emission redshift of this source is 0.541. The Mg II BAL is at a redshift of 0.524. The absorption line has an ejection velocity of 1800 km s^{-1} and is spread over 3500 km s^{-1}. We fitted the continuum of this source using the SDSS quasar composite spectrum as template. The equivalent width of the Mg II BAL increased between the SDSS and IGO epochs with more than 10σ significance (see Figs 4 and C6). The variation is seen in the strongest part of the absorption. There are no variations in the BAL features observed between the IGO epochs (see Tables 4 and 5). The CRTS continuum light curve for this source shows a trend of increase in magnitudes. But, the continuum has not varied significantly by more than 0.1 mag (see Fig. B2). Δm values for this source has a median at 0.01 with a scatter of 0.05 mag. But, in comparison with the SDSS transformed V magnitudes, the continuum flux decreased significantly(by 0.5 mag). Therefore, it seems even in this source, absorption line variability follows the variations in the continuum. As the optical depth has varied over the full profile, one cannot rule out the possibility of the optical depth variation being triggered by the continuum variation of the QSO in this case.

A4 SDSS J0944+0625

This source at $z_{em} \sim 0.6949$ has emission lines from Mg II, Hβ and Hγ. There is a broad Mg II absorption line. The strongest BAL absorption line is at a redshift of 0.6529 and has a maximum velocity of 8500 km s^{-1}. Continuum is dominated by Fe emission. We fitted the continuum with an Fe emission template. The broad dip (see Figs 4 and C7) in the higher velocity edge of the Mg II absorption could well be a part of the Fe emission optical-UV SED. So, we do not include this region while measuring the equivalent width or integrated ratio to check the variability. Here, again there are variations in the Mg II absorption line depth between different epochs (see Tables 4 and 5). As compared to the SDSS, the Mg II BAL weakened in 2008. Between 2008 and 2009 there is not much variation. But, in 2010 and 2011, the BAL weakened further. The maximum absorption line variation is seen between the SDSS and the 2010 epochs with 15σ significance for the equivalent width variation. The

CRTS light curve (in Fig. B2) shows an initial brightening followed by a steady decrease in the continuum flux by 0.1 mag in the IGO epochs. The magnitudes did not change between 2008 and 2009, but steadily decreased after 2009. As compared to the SDSS epoch, the QSO has brightened by 0.1 mag in the IGO 2008 epoch. Magnitude differences have a median of 0.04 and a standard deviation of 0.04. The $\Delta m - \Delta t$ slope is negligible. Between the SDSS and IGO epoch, the source brightened whereas the BAL weakened. Between the IGO epochs, the source weakened in the continuum flux while the BAL continued to weaken. As the equivalent width variation is monotonically decreasing whereas the continuum light curve is curved, we can probably rule out the BAL variability being driven by ionization changes.

A5 SDSS J0952+0257

This source ($z_{em} \sim 1.355$) has BALs ($z_{abs} \sim 1.300$) from Al III and Mg II. Continuum has significant contribution from iron emission lines. Hence, we fitted the optical-UV SED with a Fe emission template. Mg II and Al III lines span a velocity widths of ~ 8500 km s^{-1} and 5700 km s^{-1}, respectively. Some part of the highest velocity Mg II BAL is contributed by features in the Fe emission lines. Small variations are seen in the Mg II and Al III between the SDSS and IGO epochs. In all the IGO epochs, both Mg II and Al III weakened slightly as compared to the SDSS epoch with more than 3σ significance (see Table 4 and Fig. 4). There are no significant variations within the IGO epochs. Both Mg II and Al III varied in the same direction. For this QSO, Δm has a median of -0.03 and standard deviation of 0.06. The $\Delta m - \Delta t$ slope is -0.002 ± 0.007 mag yr^{-1}. From the light curve in Fig. B3, it is clear that the continuum flux has not changed much between different IGO observations. As compared to the SDSS epoch, the QSO brightened by 0.1 mag in the IGO epoch 2008. In this source, between the SDSS and IGO epochs, the Mg II BAL weakened when the QSO flux increased and between the IGO epochs, the Mg II BAL remained constant while the continuum light curve shows initial brightening followed by a mild fading trend. As the optical depth variations are seen over the full absorption profile, one will not be able to rule out the ionization changes causing the line variability in this source.

A6 SDSS J1208+0230

The source contains emission lines from Mg II and Al III at an emission redshift of 1.179. In addition to a broad Mg II absorption, the spectra contains a narrow Mg II absorption at $z_{abs} \sim 0.6679$. The associated Fe II and Al III lines are redshifted below the spectral range covered. Strongest BAL component is at a redshift 1.0671. The BAL is stronger at the high-velocity end and has a maximum ejection velocity and velocity spread of 18 000 km s^{-1} and 3600 km s^{-1}, respectively. As the continuum of this source is dominated by strong Fe II emission, we fitted the continuum with the template spectrum of a strong Fe emitting quasar. The unusual feature in this source is that the Mg II emission line is comparatively narrower. The Mg II absorption strength has reduced in the IGO data as compared to the SDSS (see Fig. 4). Maximum variation is seen between the SDSS epoch and the IGO 2011 epoch with 5σ significance in the equivalent widths (see Tables 4 and 5). It is also evident from Fig. 4 that the variation in Mg II profile is not uniform. The centroid of the Mg II absorption is blueshifted by about 320 km s^{-1} between SDSS and IGO 2011 epoch. The CRTS light curve for this QSO, while showing a gradual decrease in magnitudes, shows that the continuum flux of this source has not varied significantly (i.e. >0.1 mag) between our

observation period. But, it has brightened by 0.2 mag between SDSS and IGO epochs. Magnitude differences have a median of 0.04, standard deviation of 0.03 and a slope of -0.032 ± 0.004 mag yr^{-1}. Although the light curve shows a trend of decrease in the continuum flux within IGO epochs, no continuum variations ≥ 0.1 mag are observed. The Fe III and Al III emission lines have weakened significantly between the SDSS and IGO epochs. Again in this source, the absorption lines weakened when the QSO continuum brightened in flux. However, profile shape variation noted above suggests that the ionization change may not be the sole reason for the changes in Mg II optical depth in this source.

A7 SDSS J1333+0012

Variation in this source has already been reported in our previous paper (Vivek et al. 2012a). There is dynamical evolution of two components of Mg II absorption in this source. The red component (at a velocity of 1.7×10^4 km s^{-1}) completely disappeared and a blue component (at a velocity of 2.8×10^4 km s^{-1}) emerged and disappeared during our observation campaign. Significant changes are also seen in the continuum light curve. The QSO first brightened significantly between SDSS and IGO 2008 epochs, reached a maximum flux in 2009 and dimmed thereafter. A similar but opposite trend is seen in the column densities of the BALs (see fig. 2 of Vivek et al. 2012a). The observed variability is best explained by a motion of absorbing clouds across the line of sight.

A8 SDSS J2215−0045

This source is a FeLoBAL QSO where dramatic variation in the absorption lines has been reported in our recent paper (Vivek et al. 2012b). The spectrum has absorption lines from Mg II, Al III, C IV and Fe III fine structure lines. No line from Fe II is detected. Observed optical depths suggested inverted population ratios for the two Fe III fine structure lines, Fe III UV 34 and Fe III UV 48. Optical-

UV SED fitting using a quasar template having significant iron emission revealed that the observed inverted optical depths result from the over/underestimation of optical depths due to features in the iron emission at these wavelengths. All the absorption lines, except C IV, showed significant variations in the optical depth between the SDSS and IGO epochs. No variations are seen within IGO epochs. The continuum light curve for this source also shows significant changes in the flux. The quasar brightened significantly by more than 0.4 mag after the SDSS epoch. The Δm values are distributed around a median of -0.01 with a scatter of 0.2 mag and the slope of magnitude variations with elapsed time is -0.123 ± 0.009 mag yr^{-1}. This source shows maximum variations in the continuum flux among our sample. The observed variations in the BAL can be both explained by changes driven by continuum variations or by clouds moving across the line of sight (see Vivek et al. 2012b, for details).

SUPPORTING INFORMATION

Additional Supporting Information may be found in the online version of this article:

Appendix B. CRTS light curves.
Appendix C. Spectral comparison. (http://mnras.oxfordjournals.org/lookup/suppl/doi:10.1093/mnras/stu288/-/DC1).

Please note: Oxford University Press is not responsible for the content or functionality of any supporting materials supplied by the authors. Any queries (other than missing material) should be directed to the corresponding author for the article.

This paper has been typeset from a TEX/LATEX file prepared by the author.